JPET Fast Forward. Published on June 30, 2005 as DOI: 10.1124/jpet.105.088039

Vascular Binding, Blood Flow, Transporter and Enzyme Interactions on the Processing of Digoxin in Rat Liver

Lichuan Liu, Ernie Mak, Rommel G. Tirona, Eugene Tan, Phyllis M. Novikoff, Pijun Wang, Allan W. Wolkoff, and K. Sandy Pang

Departments of Pharmaceutical Sciences (L.L., E.M., R.G.T., E.T., K.S.P.) and Pharmacology (K.S.P.), University of Toronto, Toronto, Canada M5S 2S2,

and

Departments of Pathology (P.M.N.), Medicine (P.W., A.W.W.), and Anatomy and Structural Biology (A.W.W.), Albert Einstein College of Medicine, Bronx, NY 10461, USA

JPET Fast Forward. Published on June 30, 2005 as DOI: 10.1124/jpet.105.088039
This article has not been copyedited and formatted. The final version may differ from this version.

Running Title: Determinants of digoxin clearance by rat liver

Correspondence: Dr. K. Sandy Pang

Faculty of Pharmacy

University of Toronto

19 Russell Street

Toronto, Ontario

Canada M5S 2S2

E-mail: ks.pang@utoronto.ca

TEL: 416-978-6164

FAX: 416-978-8511

Text: 26 pages

Abstract: 249 words

Introduction: 657 words

Discussion: 1298 words

Tables: 6

Figures: 14

References: 40

Abbreviations: Oatp2, rat organic anion transporting polypeptide 2; Cyp3a, rat Cytochrome P450 3a; KHB, Krebs Henseleit bicarbonate buffer; PBPK modeling, physiologically-based pharmacokinetic modeling

Review Section: Absorption, Distribution, Metabolism, & Excretion

JPET Fast Forward. Published on June 30, 2005 as DOI: 10.1124/jpet.105.088039
This article has not been copyedited and formatted. The final version may differ from this version.

ABSTRACT

The roles of transporters and enzymes as determinants of the clearance of digoxin were examined in the rat liver. Digoxin is metabolized by Cyp3a and utilizes the organic anion transporting polypeptide 2 and P-glycoprotein for influx and excretion, respectively. Uptake of digoxin was found to be similar among rat periportal (PP) and perivenous (PV) hepatocytes isolated by the digitonin-collagenase method. The K_m's for uptake were 180±112 and 390±406 nM, the V_{max}'s were 13±8 and 18±4.9 pmol/min/mg protein, and the nonsaturable components were 9.2±1.3 and 10.7±2.5 μl/min/mg for PP and PV, respectively. The evenness of distribution of Oatp2 was confirmed by Western blotting and confocal immunofluorescent microscopy. When digoxin was recirculated to the rat liver preparation in Krebs Henseleit buffer (KHB) for three hours in absence or presence of 1% bovine serum albumin (BSA) and 20% red blood cell (rbc) at flow rates of 40 and 10 ml/min, respectively, biexponential decays were observed. Fitted results based on compartmental analyses revealed a higher clearance (0.244±0.082 ml/min/g) for KHB-perfused livers over the rbc-alb-perfused livers (0.114±0.057 ml/min/g) (P<0.05). We further found that binding of digoxin to 1% BSA was modest (unbound fraction = 0.64), whereas binding to rbc was associated with slow on (0.468±0.021 min^{-1}) and off (1.81±0.12 min^{-1}) rate constants. We then utilized a zonal, physiologically-based pharmacokinetic model to show that the difference in digoxin clearance was attributed to binding to BSA and rbc and not to the difference in flow rate, and that clearance was unaffected by transporter or enzyme heterogeneity.

JPET Fast Forward. Published on June 30, 2005 as DOI: 10.1124/jpet.105.088039
This article has not been copyedited and formatted. The final version may differ from this version.

INTRODUCTION

Digoxin, an important cardiotonic drug of narrow therapeutic index, is cleared by both the kidney and liver, and exhibits a long half-life in vivo due to the large volume of distribution (Rodin and Johnson, 1988). In the rat liver, digoxin is primarily metabolized by cytochrome P450 3a to the di- and mono- digitoxosides as well as digitoxigenin (Harrison and Gibaldi, 1976; Salphati and Benet, 1999), and is excreted unchanged into bile by the 170 kDa drug efflux pump, P-glycoprotein (Pgp) encoded by the multidrug resistance protein 1 (Mdr1) gene (Schinkel et al., 1995). The transport of digoxin into hepatocytes is by both passive diffusion and the rat organic anion transporting polypeptide 2 (Oatp2) which was expressed in *Xenopus laevis* oocytes (Noé et al., 1997; Guo and Klaassen, 2001; Hagenbuch et al., 2001) or LCC-PK1 cells (Shitara et al., 2002), and OATP-8 in man (Kullak-Ublick et al., 2001). Other members of the rodent and human OATP family, OATP-A, OATP-B, and OATPC (Noé et al., 1997, Hsiang et al., 1999, Kullak-Ublick et al., 2001) or members of the organic anion transporter (OAT) family (Kusuhara et al., 1999) do not transport digoxin. Significant interactions have been reported for digoxin and other drugs (Okudaira et al., 1988; Rodin and Johnson, 1988; Fromm et al., 1999), and many are attributed to the inhibition of Pgp-mediated efflux that can drastically increase drug accumulation in the brain (Schinkel et al., 1995). Hence, much attention has been devoted to adverse reactions arising from the concomitant administration of drugs with digoxin. Interactions of uptake of digoxin by rifampin, an Oatp2 inhibitor, had led to decreased digoxin clearance in the recirculating liver preparation (Lau et al., 2004), a finding that is consistent with reduced influx (Liu and Pang, 2005). Quinidine, an inhibitor of Pgp, resulted in greater metabolism and an increase in total digoxin clearance in the recirculating liver preparation (Lau et al., 2004); the increased in total hepatic clearance is inconsistent with reduced biliary excretion of the drug (Liu and Pang, 2005).

What are the other factors that may cause unexpected changes in digoxin clearance? One such factor may be transporter/enzyme heterogeneity. Another one is that basolateral efflux was altered unexpectedly when metabolic or Pgp inhibitors were used. It has been recognized that the metabolism of digoxin by CYP3a mostly occurs in the perivenous or centrilobular region of the rat liver (Oinonen and Lindros, 1995). Transporter localization studies further suggested that the distribution of Oatp2 was predominantly perivenous (PV) (Reichel et al., 1999), an observation that contrasts to that for the rat Oatp1 (Berkwerk et al., 1996; Abu-Zahra et al., 2000).

In this paper, we re-examined the lobular distribution of Oatp2 and Pgp in enriched periportal (PP) and perivenous (PV) hepatocytes prepared from rat liver. Additionally, other determinants of hepatic drug clearance were assessed. For example, binding exerts an inhibitory effect on clearance (Pang and Rowland, 1977). Modest plasma protein binding (Belz et al., 2001) but a high distribution of digoxin into red blood cell (rbc) (Hinderling, 1984) have been reported, and the slow efflux from rbc further constitutes an impediment to drug removal (Goresky et al., 1975). Blood flow rate is another factor that affects clearance (Pang and Rowland, 1977). To address the factors of binding and flow rate, digoxin binding was studied in vitro, and digoxin clearances were compared in rat liver preparations perfused with Krebs Henseleit buffer (KHB) at 40 ml/min in the absence of bovine serum albumin (BSA) and rbc, and with KHB containing 1% BSA and 20% rbc at 10 ml/min. The recirculating design was chosen since a low hepatic clearance is predicted from the modest metabolic intrinsic clearance (V_{max}/K_m or 362 pmol/min/mg/125 μM or 0.13 ml/min/g) (Salphati and Benet, 1999). We then fit the perfusion data to the compartmental and physiologically-based, pharmacokinetic (PBPK) zonal liver models. The rate-limiting condition for tracer [^{3}H]digoxin elimination: blood flow rate, vascular binding, transporter, metabolic enzyme, or Pgp activity and their accompanying heterogeneity were examined.

JPET Fast Forward. Published on June 30, 2005 as DOI: 10.1124/jpet.105.088039
This article has not been copyedited and formatted. The final version may differ from this version.

MATERIALS AND METHODS

Materials

[^{3}H]Digoxin (specific activity 19 Ci/mmol) and [^{14}C]sucrose (specific activity 6.4 mCi/mmol) were purchased from Perkin Elmer Canada (Mississauga, ON). [^{3}H]Digoxin was 94% radiochemically pure as found by high-pressure liquid chromatography (gradient of 18-28% acetonitrile and water). Unlabeled digoxin (Dg3) was obtained from Sigma Aldrich, Canada (Mississauga, ON); Dg2 (digitoxigenin bis-digitoxoside), Dg1 (digitoxigenin mono-digitoxoside), and Dg0 (digitoxigenin) were kind gifts from Dr. Emil Lin, University of California, San Francisco. Collagenase Type II was obtained from Worthington Biochemical Corporation, Lakewood, NJ. All other reagents and solvents were of HPLC grade.

Digoxin Transport

Preparation of zonal rat hepatocytes. Male Sprague-Dawley rats (301 ± 12 g; Charles River Canada, St Constant, QC) were used. The rats were kept under a 12:12 h light:dark cycle and given food and water *ad libitum*. Studies were conducted in accordance to protocols approved by the Animal Committee of the University of Toronto. Enriched PP (zone 1) and PV (zone 3) hepatocytes that were used for the transport studies and Western blot analysis were isolated by the digitonin/collagenase perfusion technique of Lindros and Pentïlla (1985), with modifications (Tirona et al., 1999). Viability of the zonal hepatocytes exceeded 97 ± 2.2 %, as assessed by trypan blue exclusion. All buffers were pre-gassed with Carbogen (95% O_2, 5% CO_2 v/v, Canox Gas, Mississauga, ON, Canada). The enrichment of PP and PV cells was confirmed by use of enzyme markers; alanine aminotransferase (PP:PV ratio of 1.9 ± 0.7) was assayed by a Sigma diagnostics kit, and glutamine synthetase (PP:PV ratio of 0.029 ± 0.039) was measured by a standard UV method (Meister, 1985).

JPET Fast Forward. Published on June 30, 2005 as DOI: 10.1124/jpet.105.088039
This article has not been copyedited and formatted. The final version may differ from this version.

Digoxin uptake by zonal hepatocytes. After pre-incubation in an atmosphere of Carbogen for 10 min at 37^{o}C, 100 µl of a mixture of unlabeled digoxin, [^{3}H]digoxin and [^{14}C]sucrose (an extracellular marker) in Krebs Henseleit bicarbonate (KHB) buffer was added to 0.5 ml of hepatocyte suspension (2 x 10^{6} cells/ml in KHB, 5 mM glucose, and 1 mM HEPES) to result in 0.08 to 3.7 µM digoxin, 3.5 to 4.4 x 10^{6} dpm/ml [^{3}H]digoxin, and 0.88 to 0.9 x 10^{6} dpm/ml [^{14}C]sucrose. Samples (100 µl) of the incubation mixture were retrieved at 15-sec intervals for up to 60 sec and immediately centrifuged across the silicon oil layer (100 µl of density 1.02 g/ml) into the bottom layer of 50 µl of 3N NaOH (Tirona et al., 1999). The tip, containing the hepatocyte pellet in 3N NaOH, was removed into a 20 ml glass scintillation vial and left overnight. After the addition of 50 µl of 3N H_2SO_4 to neutralize the base, the cellular content of [^{3}H]digoxin (dpm/mg protein) was determined by liquid scintillation spectrometry (Beckman Canada, Model 5801) after the addition of 10 ml scintillation fluor (Ready Protein, Beckman Coulter Canada, Mississauga, ON, Canada). The extracellular volume (mean value of 0.95 ± 1.4 µl) entrapped in the cellular compartment, found by the [^{14}C]sucrose content, was used as a correction factor in the determination of cellular contents. The specific activity was used to calculate the rates of uptake. Protein content in the cell suspension was measured by the method of Lowry et al. (1951).

Western blot analysis of Oatp2, Oatp1, and Pgp in rat zonal hepatocytes. About 30 ml ice cold 0.1 M Na_2CO_3 and protease inhibitors were added to the pelleted, zonal hepatocytes in a 50 ml conical tube for preparation of the crude membrane fraction. The cell suspension was homogenized at 4 °C and then centrifuged at 4 °C at 100,000*g* for 1 h. The supernatant was discarded and the pellet was kept frozen overnight at –80 °C before being sonicated for 10-30 sec in ice cold PBS (200-400 µl) in Eppendorf tubes. Protein determination was performed by the BioRad method (Richmond, CA). Western blotting was performed to determine the relative expression levels of Oatp2 and Pgp in PP and

PV hepatocyte membranes. Oatp1, shown to be present homogeneously in rat liver (Abu-Zahra et al., 2000), was also examined in the same sample to serve as a comparison for Oatp2. About 25 μg (Oatp2 and Oatp1) or 20 μg (Pgp) protein, in the same volume sample buffer, was heated at 100 °C for 7 min. Immunoblot was conducted with SDS-polyacrylamide gel electrophoresis (10% gel), and proteins were electrophoretically transferred to polyvinylidene difluoride membranes (Millipore, Boston, MA). After blocking with nonfat milk solution, the membrane was incubated with antibody for 4 h before developing for luminescent detection (Amersham, Little Chalfont, Buckinghamshire, UK). For the immunodetection of Oatp2, 1:10,000 dilution of the primary rabbit polyclonal antibody towards Oatp2 [antibody was made corresponding to amino acids 650-661 at the carboxy terminus (CTEVLRSKVTED)] and 1:20,000 dilution of the secondary antibody, HRP-anti rabbit IgG (Bio-Rad, Richmond, CA), were used. For the immunodetection of Oatp1, a 1:2,500 dilution of the primary rabbit polyclonal antibody towards Oatp1 [antibody was made to the peptide corresponding to amino acids 645-657 near the carboxy terminus (EKESEHTDVHGSP)] and 1:20,000 dilution of the secondary antibody, HRP-anti rabbit IgG (Bio-Rad), were used. Both primary antibodies were raised to the KLH-linked peptide (Bergwerk et al., 1996). For immunodetection of Pgp, a 1:333 dilution of the primary mouse monoclonal antibody C219 (Signet Laboratories, Dedham, MA) and 1:20,000 dilution of the secondary antibody, HRP-anti mouse IgG (Bio-Rad), were used.

Immunofluorescent confocal microscopy. Immunofluorescence localization and confocal microscopy were performed as previously described, with modificatons (Novikoff et al., 1996; Bergwerk et al., 1996). The liver was fixed in two ways: 1) perfusion through the portal vein with 4% paraformaldehyde/PBS and then slicing the fixed liver into sections approximately 1 to 2 mm thick with further fixation by immersion; and 2) by slicing the unfixed liver tissue into sections approximately 1-2 mm thick and immersing the sections into the fixative. The fixed liver sections were then further sectioned with a microtome to obtain 10-20 μm sections which were then sequentially

treated as follows: sodium borohydride, blocking serum, primary specific antibody (either to polyclonal anti-Oatp1 or anti-Oatp2), and fluorescent-labeled secondary antibody. Confocal microscopy was employed to image the distribution of Oatp1 [previously described in the rat liver (Bergwerk et al., 1996)] and Oatp2. Controls included microscopic examination of sections for autofluorescence and after substitution of the primary specific antiserum with nonspecific, primary serum.

Albumin Binding and rbc Distribution of Digoxin

Protein binding was conducted by equilibrium dialysis at digoxin concentrations of 10 to 100,000 nM (containing [^{3}H]digoxin) in 1% or 2% albumin in perfusate. Preliminary studies had suggested that 4.5 h was required for equilibration between the buffer and plasma (drug containing) compartments. The free or unbound fraction in perfusate plasma was given by the ratio of [^{3}H]digoxin in buffer to drug-plasma compartment.

Rbc influx of digoxin and equilibration between plasma and rbc were examined. [^{3}H]digoxin and unlabeled digoxin were incubated in 1% albumin perfusate (without rbc) at 37º C for 30 min. Then an equal volume of 40% rbc-1% albumin perfusate was added to result in digoxin concentrations of 20 to 20,000 nM in 20% rbc-1% albumin perfusate. The mixture was incubated in a rotating incubator at 37 ºC, and samples were retrieved and rapidly centrifuged to provide plasma during the next 20 min. The hematocrit (Hct) in the samples was determined. The [^{3}H]digoxin contents in the original, plasma sample and for the 20% rbc (end sample) blood perfusate were assayed by a simple precipitation procedure with acetonitrile; a set of standards containing varying known amounts of [^{3}H]digoxin were processed under identical conditions to provide the calibration curve. [^{3}H]Digoxin in plasma was assayed directly by liquid scintillation spectrometry (Beckman Coulter, Model 5801, Mississauga, ON, Canada).

Recirculating Rat Liver Perfusion

Livers (9.1 to 13.8 g) from male Sprague-Dawley rats (Charles River Canada, St Constant, QC, Canada; 290 to 360 g) were perfused in situ with recirculation of the perfusate. The animals were housed in accordance with approved protocols of the University of Toronto Animal Committee, kept under artificial light on a 12:12 h light-dark cycle, and were allowed free access to water and food *ad libitum*. Rat liver perfusion was carried out at 37 °C as previously described (Tirona and Pang, 1996), with perfusate entering *via* the portal vein and exiting *via* the hepatic vein. Perfusate of varying composition was used: one consisted of KHB and 17 mM glucose (absence of rbc and albumin), and the second contained bovine erythrocytes (20% rbc), freshly obtained and washed (a kind gift of Ryding Meats, Toronto, ON, Canada), 1% BSA and 17 mM glucose (Travenol Labs, Deerpark, IL) in KHB solution, pH 7.4. The perfusate was oxygenated with 95% oxygen-5% carbon dioxide (Matheson Gas Company, Mississauga, ON, Canada). Two reservoirs were used for study. Reservoir 1 was used for equilibration of the liver whereas Reservoir 2 contained tracer concentrations of digoxin (initial concentration 256,600 ± 105,000 dpm/ml or 6.1 ± 2.5 nM in 150 or 200 ml volume) for recirculation of the liver. Perfusate samples (1 ml) were retrieved from Reservoir 2 at 0, 2.5, 7.5, 12.5, 17.5, 22.5, 27.5, 35, 45, 55, 75, 105, 135, 165 and 180 min after initiation of perfusion. Bile was drained into pre-tared collection vials at the interval, 0-5, 5-10, 10-15, 15-20, 20-25, 25-30, 30-40, 40-50, 50-60, 60-90, 90-120, 120-150, 150-180 min, such that the midpoint times coincided with the times for perfusate samplings. A sham experiment was also conducted in absence of a liver to ascertain the extent of binding of [^{3}H]digoxin to the tubing of the perfusion apparatus; none was found.

Assay of Radiolabeled Digoxin (Dg3) and Metabolites

Digoxin (Dg3 or digitoxigenin tri-digitoxoside), digitoxigenin bis-digitoxoside (Dg2) and other metabolites monodigitoxoside (Dg1) and the aglycone (Dg0) were quantified by HPLC. The HPLC procedure of Salphati and Benet (1999) was modified to separate radiolabeled Dg3 and all of the

metabolites, Dg2, Dg1 and Dg0, within the same HPLC run. The chromatographic system (Shimadzu Corporation, Kyoto, Japan) consisted of two LC-10AT pumps, a SCL-10A system controller, a GT-104 degasser, FCV-10AL low-pressure mixing chamber, SIL-10A auto-injector, a SPD-10A UV detector set at 220 nm, and a Waters C_{18} μbondapak reverse-phase column (3.9 x 300 mm; particle size, 10 μm) and guard column (2.2 x 0.34 cm i.d.; particle size, 37-55 μm). A binary gradient consisting of water and acetonitrile was used. The initial condition of 18% acetonitrile was maintained at a flow rate of 1 ml/min. At 8 min, a linear gradient was used to increase the acetonitrile to 28% over the next 5 min, then kept there for 12 min, and was gradually returned to the original condition (18% acetonitrile) over 2 min and kept there for the next ten minutes. Radiolabeled Dg3 and its metabolites eluting at the various intervals were predetermined upon determination of the 1-min radioelutions into 7-ml minivials. Five ml of scintillation cocktail (Ready Safe, Beckman) was added to each vial, and the radioactivity was quantified by a two-channel liquid scintillation spectrophotometer (Beckman, Model 5801). The emerging radiolableled peak that was invisible due to the high specific activity of Dg3 was similar to those of the authentic standards; the run time was 37 min, and the retention times were: Dg3, 28 min; Dg2, 23 min (Figure 1).

KHB perfusate samples were centrifuged, then 100 μl was used for direct counting and 180 μl was directly injected into the HPLC. A longer procedure was used to assay the blood perfusate samples. Unlabeled digoxin (25 nmole) was added to blood perfusate (400 μl) as an internal standard. Then 2400 μl acetonitrile was added and the mixture was mixed well for deproteinization. After centrifugation, the supernatant was removed into a fresh glass tube and dried under nitrogen. The residue was dissolved in 120 μl mobile phase (25% acetonitrile, 75% ddH_2O), and the reconstituted sample was centrifuged again before 60 μl was injected into the HPLC. Standards for calibration curves (varying amounts of [^{3}H] digoxin) were processed under identical conditions. Bile was diluted

with ddH_2O, and an aliquot was injected into the HPLC. Another aliquot of the diluted bile sample was counted directly. The extent of excretion of Dg3 and its metabolite(s) was quantified by the fractional dpm of the species in the sample times the total counts of the sample.

Calculations and Modeling

Transport studies. The cumulative amounts of digoxin (pmol/mg protein) that were taken up (after correction for the entrapped extracellular component) into hepatocytes within the first minute were regressed against the corresponding incubation time. The slope yielded an initial uptake rate, v. Upon presenting the rate, v, against [S], the substrate concentration, the data were fit to various curve models (general equation shown as Equation 1), for a single saturable component, for the sum of one saturable and one nonsaturable component, for two saturable components, or two-saturable components plus a nonsaturable component. The general equation describes the various saturable systems which are characterized by the $V_{max,i}$ and $K_{m,i}$, or the maximum capacity and Michaelis-Menten constant for each i^{th} saturable component, and a linear (nonsaturable) component for uptake, PS_{uptake}. The nonsaturable component for digoxin represents most likely passive diffusion for this lipophilic substrate.

$$v = \sum \frac{V_{max,i}[S]}{K_{m,i} + [S]} + PS_{uptake}[S] \qquad (1)$$

Rbc partitioning and plasma protein binding. The model that describes the exchange of digoxin between plasma and rbc in relation to the hematocrit (Hct) is shown in Figure 2. The blood concentration was estimated as the initial plasma concentration/2 when equal volumes of blank blood (40% rbc, 1% BSA) and plasma (1% BSA) were mixed. The concentration of digoxin in rbc was assessed from mass balance, knowing the concentration of drug in blood (C_b), in plasma (C_p) and the hematocrit.

JPET Fast Forward. Published on June 30, 2005 as DOI: 10.1124/jpet.105.088039
This article has not been copyedited and formatted. The final version may differ from this version.

$$C_{rbc} = \frac{C_b - C_p (1 - Hct)}{Hct} \quad (2)$$

The unbound concentration in plasma, f_p, is the ratio of unbound to total drug in plasma.

Only the unbound species of digoxin in rbc and plasma are assumed to undergo equilibration. The on and off rate constants, k_{pr} and k_{rp}, respectively, denote the rate constant for movement of unbound digoxin from plasma to rbc, and from rbc to plasma. Inasmuch as the binding of digoxin to rbc was uncertain, a modified rate constant, k'_{rp}, that equals the product f_{rbc} k_{rp}, was used.

The rates of change of digoxin concentrations in rbc (C_{rbc}) and plasma (C_p) are,

$$\frac{dC_{rbc}}{dt} = k_{pr} f_p C_p \frac{(1 - Hct)}{Hct} - k'_{rp} C_{rbc} \quad (3)$$

$$\frac{dC_p}{dt} = k'_{rp} C_{rbc} \frac{Hct}{(1 - Hct)} - k_{pr} f_p C_p \quad (4)$$

and the unbound fraction in blood (f_b) is related to the unbound fractions in rbc (f_{rbc}) and f_p as shown below (Pang and Rowland, 1977), with the assumption that there is no concentrative transport of drug into the rbc.

$$f_{rbc} = \frac{Hct}{\frac{1}{f_b} - \frac{1 - Hct}{f_p}} \quad (5)$$

The terms, k'_{rp} and k_{pr}, have been shown to be related to the concentration ratio of rbc to plasma,

$$\frac{C_{rbc}}{C_p} = \frac{k_{pr}(1 + \gamma)(1\text{-}Hct) f_p}{Hct\ k'_{rp}} \quad (6)$$

where γ is the ratio of the interstitial or Disse space to the sinusoidal plasma space (Pang et al., 1988).

Rat liver perfusion studies. Model-independent methods were used to calculate clearances. The area under the curve (AUC) of Dg3 in perfusate was calculated by trapezoidal rule and extended to time infinity (concentration of last sample/elimination rate constant) to estimate the total clearance, $CL_{liver,tot}$, by dose/AUC in both sets of studies. The cumulative amount of Dg3 excreted in bile over 3 h was summed and expressed as %dose; The amounts of Dg2 in bile and perfusate at the same time point were summed and the cumulative amount at 165 min was expressed as %dose. However, this amount would underestimate the total amount of Dg2 metabolite formed since minor levels of Dg1 and Dg0 were detected and not all of the metabolites formed appeared in bile and perfusate; Dg2 and other metabolites may be trapped within the liver. The total recovery as Dg2 and Dg3 in bile and perfusate accounted for only 50-55%, and a substantial amount of radioactivity was indeed found in the liver at 180 min.

Compartmental modeling. Compartmental models, either with elimination from the central compartment (Figure 3A) or peripheral compartment (Figure 3B), were used for fitting of Dg3 perfusate and bile data. Both models are equally consistent to describe the biexponential decay of Dg3 in perfusate. Since the summed amounts of Dg2 appearing in perfusate and bile may not represent total metabolism due to residual [^{3}H]-radioactivity in liver, the summed Dg2 amount was not used for fitting. Rather, the rate constant for metabolism k_m, [as ($k_{10} - k_e$) or ($k_{20} - k_e$)] and the total amount of metabolite formed were estimated from modeling (Figure 3).

PBPK zonal liver modeling. For the description of data based on the physiological variables, a physiologically-based pharmacokinetic (PBPK), zonal model consisting of three compartments in series to represent zones 1, 2, and 3 in the liver (Tirona and Pang, 1996; Abu-Zahra and Pang, 2000) was used (Figure 4). In this model, physiological variables such as flow rate and tissue and blood volumes were used. Moreover, the PBPK, zonal model encompasses zonal transport, metabolism, and excretion of Dg3 in the PP, midzonal and PV regions (Figure 4A) as well as rbc binding, namely, the

JPET Fast Forward. Published on June 30, 2005 as DOI: 10.1124/jpet.105.088039
This article has not been copyedited and formatted. The final version may differ from this version.

transport into and out of red cells, and albumin binding (Figure 4B) in the rat liver preparation. It is assumed that the free species is the one that is transported, metabolized, or excreted. This model describes heterogeneity in basolateral influx transport, denoted as CL_{in1}, CL_{in2}, and CL_{in3} within zones 1, 2, and 3, respectively. Similarly, CL_{ef1}, CL_{ef2}, and CL_{ef3} are the clearances for basolateral efflux, $CL_{int,sec1}$, $CL_{int,sec2}$, and $CL_{int,sec3}$ for biliary excretion, and $CL_{int,met1}$, $CL_{int,met2}$, and $CL_{int,met3}$ for metabolism within zones 1, 2, and 3, respectively.

Fitting

The program SCIENTIST v.2 (MicroMath Scientific Software, Salt Lake City, Utah) was used for all fittings and simulations. Fitting was performed with various weighting schemes of unity, 1/observation and 1/observation^2. Model selection criterion (MSC), a modified Akaike information criterion (AIC), was used as a discriminator for the optimal model.

Hepatocyte uptake. Equtaion 1 was used for fitting of the digoxin uptake data. The total uptake clearance (CL_{uptake}) under first-order conditions was given by the ratio, $V_{max,i}/K_{m,i}$, of the various transporter systems + the nonsaturable uptake clearance.

Rbc and albumin binding. Data for plasma protein binding were used to estimate the unbound fraction (f_P) as unbound plasma concentration/total plasma concentration. Then data (n=3) for red cell binding were averaged, and the mean data for C_{rbc} and C_p for Dg3 blood concentrations ranging from 20 to 20,000 nM were fitted to Equations 3 and 4.

Compartmental modeling. A set of differential equations (see Appendix A) was used for data fitting to the compartmental models (Figure 3). The intercompartmental rate constants, k_{12} and k_{21}, the excretion rate constant, k_e, and k_{10} (or k_{20}) were fitted; k_m was found by difference ($k_{10} - k_e$ or $k_{20} - k_e$). The hepatic clearance ($CL_{liver,tot}$) was calculated from the derived parameters: $k_{10}V_1$ (volume of reservoir) for elimination from the central compartment, or $k_{20}V_1 \times k_{12}/(k_{21} + k_{20})$, when elimination takes place in the peripheral compartment. The biliary ($CL_{liver,ex}$) and metabolic ($CL_{liver,met}$) clearances

JPET Fast Forward. Published on June 30, 2005 as DOI: 10.1124/jpet.105.088039
This article has not been copyedited and formatted. The final version may differ from this version.

are denoted as $k_e V_1$ and $k_m V_1$, respectively, when Dg3 is eliminated from the central compartment; or $k_e V_1 \times k_{12}/(k_{21} + k_{20})$ and $k_m V_1 \times k_{12}/(k_{21} + k_{20})$, respectively, when Dg3 elimination occurs in the peripheral compartment. The hepatic extraction ratio, E, is estimated as $CL_{liver,tot}$ /flow rate.

PBPK zonal liver modeling. Data of Dg3 in reservoir and in bile were fit by mass balance differential equations for first-order conditions (see Appendix B). The designated flow rates, volumes, and hematocrit from rat liver perfusion study were known constants. The fitted parameters on the rbc partitioning (k_{pr} and k'_{rp}) and protein binding (f_p), obtained from the *in vitro* binding study, were assigned as constants. The uptake clearance, CL_{in}, was obtained by scale-up of the *in vitro* hepatocyte uptake data: the experimentally determined in vitro V_{max}/K_m, added to the nonsaturable uptake clearance, yielded 12.1 ml/min/g after scale-up for the average of the PP and PV transport data. The value was divided by three so that $CL_{in1} = CL_{in2} = CL_{in3}$ since even distribution of Oatp2 was found. An initial estimate of the total, hepatic intrinsic clearance (CL_{int}) was calculated, based on simplified equations showing below for the "well-stirred" (Equation 7) or "parallel tube" (Equation 8) model (Pang and Rowland, 1977). The equation is valid when the influx and efflux transport of digoxin across the hepatocytes membrane is fast, and metabolism and excretion are slow. The assumption is valid for Dg3. The total intrinsic clearance was divided by three to provide a crude estimation of the zonal, intrinsic clearance.

For the "well-stirred"model

$$CL = \frac{Qf_b CL_{int}}{Q + f_b CL_{int}} \quad (7)$$

For the "parallel tube"model

$$CL = Q\,(1 - e^{-f_b CL_{int}/Q}) \quad (8)$$

The basolateral efflux clearance (CL_{ef}), metabolic intrinsic clearance ($CL_{int,met}$), secretory intrinsic clearance ($CL_{int,sec}$), and the unbound tissue binding (liver tissue unbound fraction, f_t) were estimated from fitting. Each of the zonal clearances was expressed as a percent of total intrinsic clearance. For example, the metabolic activity of Cyp3a was perivenous, and could be described by 10%, 30% and 60% of the total metabolic intrinsic clearance ($CL_{int,met}$) dispersed in the periportal (zone 1), midzonal (zone 2), and perivenous (zones 3) regions, respectively. Alternately, the activities may be assigned to be evenly distributed among all three zones, that is, $CL_{int,met1} = CL_{int,met2} = CL_{int,met3} = CL_{int,met}/3$. This was assumed for Pgp as found from Western blot analysis, and each zonal secretory intrinsic clearance is $CL_{int,sec}/3$.

Simulations. The parameters obtained after fitting of data from the rbc-alb-perfusion studies (see middle column, table 4) were used for further simulations with the PBPK, zonal model shown in Figure 4B. The first set of simulations was based on an even distribution of $CL_{int,met}$, and the simulations were made to demonstrate the changes in digoxin disposition (metabolism and excretion) when the flow rate was altered from 10 to 40 ml/min, when the binding of digoxin to rbc, then to albumin was set as zero, sequentially ($k_{pr} = k'_{rp} = 0$, $f_p = 1$), and when the influx, efflux, secretory or metabolic intrinsic clearances were doubled. Only one change was made at any one time. In these simulations, the concentration-time profiles of Dg3 in perfusate, the cumulative amount in bile, and the total formation of Dg2 were simulated. The $CL_{liver,tot}$ (dose/AUC), $CL_{liver,ex}$ (total Dg3 excreted amount in bile/AUC) and $CL_{liver,met}$ (total Dg2 formation/AUC) were estimated for each condition.

To address whether or not enzyme heterogeneity and transporter heterogeneity would result in any unexplained observations in digoxin clearance, such as increased hepatic clearance upon inhibition of Pgp (Lau et al., 2004), a second set of simulations was performed. In this instance, the total activity for transport or metabolism was divided among zones 1, 2, and 3. An even distribution in zones 1, 2, and 3 (1:1:1) was designated with the distribution "A". A preferential PV distribution was assigned

(1:3:6), meaning that 10%, 30% and 60% of the total activity resided in zones 1, 2, and 3, respectively, and was assigned a "B" distribution. The reverse pattern, a preferential PP distribution (6:3:1) meaning that 60%, 30%, and 10% of the total activity resided in zones 1, 2, and 3, respectively, was assigned the distribution of "C". Each model was described by three letters, with the first letter describing the parallel distribution patterns of influx and efflux clearances (CL_{in} and CL_{ef}). The second and third letters described the distribution patterns of the metabolic ($CL_{int,met}$) and secretory ($CL_{int,sec}$) intrinsic clearances, respectively. The various distributions resulted in 27 possible combinations. All of the possible distribution patterns were used to simulate digoxin disposition with the PBPK, zonal model shown in Figure 4B. Again, the parameters from rbc-alb-perfused liver (Table 4) were used initially to evaluate the effect of zonal metabolic and transporter heterogeneity on clearance with the model. Several other sets of simulations were made to explore the effects of the relative values the intrinsic clearances, $CL_{int,met}$ and $CL_{int,sec}$, to the transport clearances, CL_{in} and CL_{ef}. Since values of the $CL_{int,met}$ and $CL_{int,sec}$ were much lower than those for CL_{in}/CL_{ef}, values of the $CL_{int,met}$ and $CL_{int,sec}$ were increased to 5-fold and 50-fold of the original values, respectively, or 100-fold and 500-fold, respectively, in order to examine the influence of enzymatic and excretory activities when these values were comparable to those for basolateral influx and efflux. Lastly, the $CL_{int,sec}$ was reduced to 10% of the original value to examine the condition of inhibition of Pgp efflux on metabolism. The concentration time-profiles for Dg3 in the reservoir, and the cumulative amounts of Dg3 in bile, as well as the total amount of Dg2 formed were used to estimate the areas under the curve, and in turn, the total, metabolic, and biliary excretory clearances. The values of the clearances according to the various distribution patterns were subsequently ranked.

Statistical analysis

For comparison of data, a one-way ANOVA was performed. The data were expressed as mean ± S.D. An alpha level of 0.05 was set as the threshold for statistical significance.

RESULTS

Uptake of digoxin by isolated, zonal rat hepatocytes. The time course for digoxin accumulation into cells (amount/mg cells *vs.* time plot) was linear over 1 min (data not shown). These values provide the initial uptake velocities of digoxin for the various concentrations used. Digoxin uptake was best described as the sum of a saturable component and a nonsaturable component (Figure 5). The K_m and V_{max} and the nonsaturable linear uptake clearance, PS_{uptake}, were obtained with the optimal weighting of 1/observation^2. Differences in parameter estimates were insignificant among PP and PV zonal hepatocytes (Table 1). The fitted K_m is low (180 and 390 nM), suggesting a high-affinity but readily saturable process, whereas the nonsaturable component was appreciable, although it constituted about 10% of the transport clearance under first order conditions. In view of the lipophilic character of digoxin, this component is most likely due to passive diffusion.

Distribution of Oatp2 and Pgp in zonal rat hepatocytes and in rat liver. The intensities of immunodetectable Oatp2, Oatp1 (Figure 6) and Pgp (Figure 7) by Western blots of PP and PV cells showed similar zonal distributions. The relative intensities of Oatp2 in PP and PV cells were 1,260 ± 423 and 1,620 ± 303 arbitrary units (525 ± 70 and 572 ± 138 arbitrary units in PP and PV cells for Oatp1), respectively ($P > 0.05$), whereas the relative intensities of Pgp in PP and PV cells were 1850 ± 700 and 2800 ± 750 arbitrary units, respectively ($P > 0.05$), suggesting that all three proteins were present homogeneously throughout the acinus of the rat liver. Confocal immunofluorescent microscopy revealed that rat Oatp2 was present in hepatocytes located in portal, midzonal and central areas of the hepatic lobule, although their appearance may not be contiguous (Figure 6). We consistently observed variable fluorescence intensities within and between the areas. The distribution of Oatp2 in rat liver was the same regardless of the fixation protocol employed. Oatp2 was distinctly

present in the PP region as well as the PV region. These results mirrored that of Oatp1, which was distributed homogeneously throughout the liver lobule (Bergwerk et al., 1996; Abu-Zahra et al., 2000).

Protein binding and red blood cell (rbc) distribution of digoxin. The unbound fraction of digoxin in plasma (f_p) from the *in vitro* binding study was 0.64 ± 0.03 (Table 2). Binding to 1% albumin was modest, and the unbound fraction was constant even when the albumin concentration was doubled to 2% (Figure 8). The fit of the rbc partitioning data (Figure 9) to the model (Figure 2) yielded values of k_{pr} (0.468 ± 0.021 min^{-1}) and k'_{rp} (1.81 ± 0.12 min^{-1}), showing that the on rate constant (k_{pr}) was lower than the apparent off rate constant (k'_{rp}) (Table 2). The unbound fraction in blood, at equilibrium, f_b, calculated as $f_p/(C_b/C_p)$, equaled 0.615.

Digoxin disposition in KHB and rbc-albumin perfused rat liver preparations. Dg3 underwent an initial rapid distribution, then a protracted decline in livers perfused with KHB at 40 ml/min, in a distinctly biexponential decay profile (Figure 10A). Only Dg2 was found in perfusate, and Dg1 and Dg0 levels were very low or non-existent (Figure 10B). Both Dg3 and Dg2 were excreted into bile in comparable quantities (Fig. 10). However, the unbound biliary clearance of Dg3 (excretion rate of Dg3/midtime unbound Dg3 concentration in perfusate or 0.05 ± 0.02 ml/min/g liver) was significantly lower ($P < 0.05$) compared to the apparent biliary clearance of Dg2 (excretion rate of Dg2/midtime Dg2 concentration in perfusate or 1.10 ± 0.72 ml/min/g liver) (plot not shown).

Comparable results were observed when Dg3 in 20%-rbc and 1%-BSA medium recirculated through the liver at 10 ml/min (Figure 11). A more shallow distribution phase of digoxin was observed in the presence of the lower flow rate and vascular binding elements such as rbc and albumin in the rbc-alb-perfused livers (Figure 11A) in comparison to the KHB-perfused livers (Figure 10A). The metabolite, Dg2, was found in perfusate, and was excreted avidly into bile; other metabolites, Dg1 and Dg0 were present at very low levels (Figure 11B). The apparent excretion clearance of Dg2 (0.44 ±

0.04 ml/min/g liver) was significantly greater ($P < 0.05$) than the unbound biliary clearance of Dg3 (0.02 ± 0.04 ml/min/g liver) (plot not shown). The hepatic clearances calculated from dose/AUC from trapezoidal method were 0.192 ± 0.049 vs. 0.123 ± 0.061 ml/min/g, respectively, for the KHB-perfused liver and rbc-alb-perfused livers ($P > 0.05$). Upon correction for f_b, the clearance values ($CL_{liver,tot}/f_b$) become virtually identical (Table 3).

Compartmental fitting. Compartmental fits of data from individual experiments and to the averaged data were performed. Fits obtained for individual experiments provide mean values (Table 3) that were similar to the parameters obtained for the fit of the average data (data not shown). For fits to the model that assumed elimination from the central compartment, no difference was found in k_{12}, k_{21}, and k_{10}, due to the large variability among the preparations; however, k_e and the total clearance (0.114 ± 0.057 vs. 0.244 ± 0.082 ml/min/g) were significantly lower for the rbc-alb- perfused livers in comparison to those for the KHB-perfused livers ($P < 0.05$). For fits to the model with elimination from the peripheral compartment, significant differences were found for k_m and k_{20}, and E ($P < 0.05$) but not for the total hepatic clearance between KHB-perfused and rbc-alb-perfused livers, regardless of correction for the unbound fraction in blood, f_b (Table 3). After normalization of $CL_{liver,tot}$ by f_b, values of $CL_{liver,tot}/f_b$ provided by compartmental fitting were similar for the KHB-perfused and rbc-alb-perfused livers, when elimination occurred from central (0.244 ± 0.082 vs. 0.185 ± 0.093 ml/min/g, $P > 0.05$) or peripheral compartment (0.198 ± 0.111 vs. 0.191 ± 0.083 ml/min/g, $P > 0.05$) (Table 3). In all of the fits, the predicted amounts of Dg2 formed were higher than the summed amount of Dg2 obtained from the perfusate and bile (Figures 10B and 11B).

Generally speaking, good fits were obtained for the models encompassing elimination from the central or peripheral compartments (Figures 10A and 11A). The biliary excretion data appeared to be better predicted during the earlier times by the peripheral compartment. But the small difference

JPET Fast Forward. Published on June 30, 2005 as DOI: 10.1124/jpet.105.088039
This article has not been copyedited and formatted. The final version may differ from this version.

(observed only with semi-logarithmic plot) failed to alter the overall fit as to whether or not removal occurred from the central or peripheral compartment. This was shown by the similar MSC values and sum of squared residuals ($P > 0.05$, Table 3). It was not possible to discern whether elimination occurred in the central or peripheral compartment. Moreover, the fit failed to reveal unequivocally the underlying reason for the difference in the clearance of digoxin estimated with compartmental modeling - binding of digoxin to BSA or rbc, or the flow rate.

PBPK zonal liver modeling. When the mean data were fit to the PBPK zonal models (Figures 4A and 4B), the CL_{ef}, $CL_{int,met}$, $CL_{int,sec}$ and f_t were found not to differ between KHB-perfused and rbc-alb- perfused livers ($P > 0.05$; Table 4). Good fits were obtained (Figures 12A and 12B), and the parameters were found to be similar regardless of whether or not heterogeneous or evenness in CL_{int,met_i} was considered (Table 4). That presence of heterogeneity in metabolic activity did not exert an effect on the overall clearance of digoxin that was poorly extracted. The digoxin removal within the liver would fail to evoke a steep sinusoidal or intracellular concentration gradient in the liver lobule. Under this condition, the enzymes are recruited in the entirety by the substrate (Pang and Stillwell, 1983), and enzymatic heterogeneity became irrelevant. When the data were forced fit to provide a common set of $CL_{int,met}$, $CL_{int,sec}$, CL_{ef}, and f_t, the fits were not as good as those when data of the KHB- and rbc-livers were fit separately (fits not shown). But generally, the parameters obtained from forced-fitting were similar to those furnished from separate fits to data of KHB-perfused and rbc-alb-perfused livers (Table 4).

Simulations with PBPK zonal liver Model

Flow or binding on digoxin clearance. The fitted parameters for the rbc-alb-perfused of $CL_{liver,tot}/f_b$ provided by compartmental fitting were similar in KHB-perfused and rbc-alb-perfused liver preparation (flow = 10 ml/min with rbc and albumin binding, middle panel of Table 4) were used for simulations. When the blood flow rate was increased from 10 to 40 ml/min, it was apparent that

JPET Fast Forward. Published on June 30, 2005 as DOI: 10.1124/jpet.105.088039
This article has not been copyedited and formatted. The final version may differ from this version.

flow failed to perturb the concentration-profile and decay processes of digoxin, and both excretion and metabolism of digoxin remained similar (Figure 13A). Whereas when red cell binding was set as nonexistent (k_{pr} = k'_{rp} = 0), the decay profile of digoxin was more rapid, and all clearance values: excretory and metabolic, were increased. When albumin binding was further set as zero (f_p = 1), steeper changes in decay were observed, and all of the clearance values were increased further (Figure 13B, Table 5).

Changes in CL_{in}, CL_{ef}, $CL_{int,met}$ and $CL_{int,sec}$. To investigate the interrelationship of the transporters and the metabolic enzymes, the intrinsic clearance, CL_{in}, CL_{ef}, $CL_{int,met}$ or $CL_{int,sec}$ was doubled in individual simulations. Upon doubling of CL_{in}, the decay of digoxin was much faster, and $CL_{liver,tot}$, $CL_{liver,ex}$, and $CL_{liver,met}$ all increased, with digoxin being more highly excreted and metabolized (Figure 14A, Table 5); whereas with a doubling of CL_{ef}, the decay of digoxin was much slower, and $CL_{liver,tot}$, $CL_{liver,ex}$, and $CL_{liver,met}$ all decreased (Figure 14B, Table 5) An increase of $CL_{int,met}$ increased $CL_{liver,met}$ and $CL_{liver,tot}$ but decreased the alternate (competing) clearance, $CL_{liver,ex}$, and the decay of digoxin was much faster (Figure 14C, Table 5). The increase in $CL_{int,sec}$ only slightly hastened the disappearance of digoxin, increasing the $CL_{liver,tot}$ slightly, although the $CL_{liver,ex}$ was increased and $CL_{liver,met}$ decreased slightly (Figure 14D, Table 5). Only small differences in excretion existed in the last two situations because metabolism was the major removal pathway of digoxin.

Transporter and enzyme heterogeneity. The clearances for the 27 combinations of zonal patterns (1:1:1, 1:3:6, and 6:3:1, denoted by A, B and C, respectively) for influx/efflux, metabolism, and secretion were estimated with simulations. The best three (highest clearances) and the worst three (poorest clearances) conditions are listed in Table 6. The best condition for total clearance $CL_{liver,tot}$ existed when the influx/efflux, metabolism, and secretion intrinsic clearances were evenly distributed (distribution pattern of AAA), and the even distribution of CL_{in}/CL_{ef}, allowed access of substrate into the cell for metabolism or excretion. The worst condition was when the CL_{in}/CL_{ef} vs. $CL_{int,met}$ or

JPET Fast Forward. Published on June 30, 2005 as DOI: 10.1124/jpet.105.088039
This article has not been copyedited and formatted. The final version may differ from this version.

$CL_{int,sec}$ exhibited opposite distributions (CBB or BCC), and persisted regardless of the values of $CL_{int,met}$ and $CL_{int,sec}$. The metabolic clearance, $CL_{liver,met}$, was highest when parallel distributions existed between CL_{in}/CL_{ef} and $CL_{int,met}$, the dominant removal pathway, and this occurred when CL_{in}/CL_{ef} or $CL_{int,met}$ displayed distribution A or C. The $CL_{liver,met}$ was lowest when $CL_{int,met}$ displayed distribution B. For the biliary clearance, $CL_{liver,ex}$, higher values existed when the $CL_{int,sec}$ exhibited distribution A or C, and when $CL_{liver,met}$ was of distribution B, representing a lower metabolic clearance. The $CL_{liver,ex}$ was lowest when the CL_{in}/CL_{ef} and $CL_{int,sec}$ were of opposite distributions (B vs C, or C vs B). These general patterns were consistent over the parameter space examined, and when the biliary intrinsic clearance was reduced to 10% of the original value (Table 6). Moreover, the varying distribution patterns of CL_{in}/CL_{ef}, $CL_{int,met,}$ and $CL_{int,sec}$ did not change the trend in the total clearance when $CL_{int,sec}$ was inhibited. The metabolic clearance was increased while the biliary and total clearances were decreased with inhibition of Pgp (effectively, a reduction in $CL_{int,sec}$).

DISCUSSION

The uptake of digoxin has been attributed to the organic anion transporting polypeptide 2 (Oatp2) in the rat liver (Noé et al., 1997; Hagenbuch et al., 2001; Shitara et al., 2002) and OATP-8 in humans (Kullak-Ublick et al., 2001) based upon transport studies performed in *Xenopus oocytes* (Noé et al., 1997; Hagenbuch et al., 2001) or LCC-PK1 cells (Shitara et al., 2002) expressing these proteins. However, we were unable to confirm Oatp2-mediated digoxin uptake in stably transfected HeLa cells in which Oatp2 expression was under control of a Zn^{2+}-activated methallothionein promoter, similar to studies we performed for rat Oatp1 (Pang et al., 1998). The observed digoxin uptake rate was high but represented nonsaturable transport that was also present in HeLa cells which had not been stimulated with Zn^{2+} (unpublished data, A. W. Wolkoff and K. S. Pang). Our failure to demonstrate that digoxin is an Oatp2 substrate may be attributed to use of mammalian cells vs. *Xenopus oocytes*. It could also be further argued that, for the mammalian LCC-PK1 cells that were transfected with rat Oatp2, the digoxin transport rates were very low and existed at levels similar to those for background transport (Shitara et al., 2002).

Expression of Oatp2, present at the basolateral plasma membrane of the rat hepatocyte (Kullak-Ublick et al., 1994; Meier and Stieger, 2002), was reported to be higher in the perivenous region (Reichel et al., 1999), as also found for Oatp4 (Cattori et al., 2001). The findings contrasted that for Oatp1 which was homogeneously distributed in rat liver (Bergwerk et al., 1996; Abu-Zahra et al., 2000). Upon induction with phenobarbital, immunoreactive Oatp2 in the perivenous region increased disproportionately over the periportal region, and hepatocyte uptake of digoxin in phenobarbital treated rats was 4-fold greater than untreated rats, a finding which was consistent with increased Oatp2 expression (Hagenbuch et al., 2001). By contrast, the distribution of Oatp2 found by Western blots in our PP and PV cells and our digoxin transport studies revealed the homogeneous presence of Oatp2 in

both PP and PV cells (Figures 5 and 6). Moreover, confocal immunofluorescence microscopy revealed that Oatp2 was present in periportal, midzonal, and perivenous cells, although the presence was spotty and not contiguous (Figure 6). All of the data suggest that Oatp2 is also present in the PP region. Moreover, the transport of digoxin, in absence or presence of inhibitors with freshly prepared PP and PV hepatocytes, was similar (Tirona et al., 2000). The extents of transport inhibition by various digoxin inhibitors among the rat zonal hepatocytes were also similar (Tirona et al., 2000). Equal extents of inhibition of digoxin uptake was observed with taurocholate, estradiol 17β-glucuronide, and bromosulfophthalein, Oatp1 or Oatp2 substrates, as well as the diuretics, bumetanide and ethacrynic acid in PP and PV hepatocytes; however, salicylate and TEA, OAT and OCT substrates, respectively, were devoid of effect (Tirona et al., 2000).

The hepatic transport of digoxin by PP and PV hepatocytes (Figure 5) showed that the saturable transport system is of high affinity (Table 1); the K_m's were similar among PP and PV hepatocytes ($P > 0.05$) and these values are similar to that found for Oatp2 by Noé et al. (1997). Upon expression of the uptake data in terms of the V_{max}/K_m + nonsaturable clearance, the values of the summed uptake clearances of digoxin for both PP and PV hepatocytes are extremely rapid, averaging about 100 μl/min/mg protein (Table 1) or 12 ml/min/g liver (Table 4). The metabolic intrinsic clearance of digoxin, derived from the K_m (125 μM) and V_{max} (362 pmol/min/mg microsomal protein) for digoxin metabolism (Salphati and Benet, 1999), is 0.13 ml/min/g liver (using the scaling factor of 44.8 mg microsomal protein per g liver), and is comparatively smaller. Because of the rapid exchange of digoxin between the sinusoid and hepatocyte at basolateral membrane (large CL_{in} and CL_{ef}), $CL_{int,sec}$ and $CL_{int,met}$ or vascular binding are important determinants of digoxin hepatic clearance. The same may be speculated for the human liver in which the metabolic intrinsic clearance of digoxin is poor, and sinusoidal transport is likely very fast due to the lipophilicity of digoxin.

In terms of modeling of the transport, metabolic, and binding data, a simplified, mathematical relationship for CL_{in}, CL_{ef}, $CL_{liver,tot}$, $CL_{liver,ex}$, and $CL_{liver,met}$ that encompasses vascular binding on organ clearance have been shown for the "well-stirred" model (Sirianni and Pang, 1997). However, it was shown the physiologically-based pharmacokinetic model (PBPK) zonal model is more apt to reveal the influence of the determinants on clearance as well as heterogeneity factors, as found for enalapril removal (Abu-Zahra and Pang, 2000; Liu and Pang, 2005). The PBPK zonal model is also superior over the compartmental model to demonstrate the pertinent factors that influence the clearance of digoxin. For example, the PBPK zonal model showed that the differential flow rates in the rbc (Q = 0.811 ml/min/g) and KHB-perfused livers (Q = 3.58 ml/min/g) played a minor role in the clearance of digoxin, a low extraction drug. Based on simulations with the PBPK zonal model, vascular binding and not flow affected the kinetics of the digoxin (Figure 13). Considering the large amounts of erythrocytes in blood, it is important to assess the effects of rbc binding/distribution on digoxin clearance (Hinderling, 1984). Because of the slow equilibrium time of digoxin between plasma and rbc (Figure 9), red cell binding is slow and will affect the equilibration time of digoxin in liver. There was slow influx of digoxin from plasma to rbc (k_{pr} of 0.468 min^{-1}) and relative rapid efflux of digoxin from rbc to plasma (k'_{rp} of 1.81 min^{-1}). This was predicted in the unbound clearance ($CL_{liver,tot}/f_b$) vs. time plot when the same parameters (forced fit) were used to simulate the amounts of Dg3 in perfusate and bile. The resultant simulated data revealed that a longer time was needed to reach the same asymptotic value for $CL_{liver,tot}/f_b$ when rbc binding exists (simulation not shown).

Moreover, the PBPK zonal, liver model better describes the heterogeneity in transporter and metabolic functions within the liver. The simulations showed general patterns for clearance estimates with heterogeneity in transporter, metabolic, and excretion activities (Table 6). The even distribution of transporters is optimal for the achievement of highest organ clearance, whereas transporter and intrinsic clearances of opposite distributions provide the poorest organ clearance. As expected, a

greater overlap in influx transporter activity and the intrinsic clearance, either for metabolism or excretion, also provides a greater metabolism or excretion. The converse is also true. The lesser overlap in influx transporter activity and the intrinsic clearances brings about decreased metabolism or excretion (Table 6). The PBPK zonal model further addresses whether decreased inhibition of Pgp would evoke increased metabolism as well as total clearance of digoxin (Lau et al., 2004). From the present simulations which mimic the inhibition of Pgp (10% $CL_{int,sec}$), zonal heterogeneity cannot account for the observation of increased clearance, although it is expected that metabolism of Dg3 should increase. The trend paralleled that of Liu and Pang (2005) who also examined these relations in a simplified, PBPK model. The clearance of Dg3 would increase when the Pgp inhibitor further decreased the basolateral efflux (Figure 14). This type of investigation, including both transport and enzyme heterogeneity (Abu-Zahra and Pang, 2000), is quantitative in revealing the determinants of clearance and the nature of competitive pathways. These concepts are universal in predicting the changes in metabolism and excretion which are competing pathways among elimination organs. Although there are the usual recognizable species differences between rat and man in terms of the transport and metabolism of digoxin in the liver (Doherty and Perkins, 1962; Wirth and Frolich, 1974), the poor hepatic clearance and metabolism, the red cell and albumin binding, and the high lipophilicity suggest a similar role of red cell and albumin binding on the hepatic clearance of digoxin in man.

REFERENCES

Abu-Zahra TN, and Pang KS (2000) Effect of zonal transport and metabolism on hepatic removal: enalapril hydrolysis in zonal, isolated rat hepatocytes in vitro and correlation with perfusion data. *Drug Metab Dispos* 28:807-813.

Abu-Zahra TN, Wolkoff AW, Kim RB, and Pang KS (2000) Uptake of enalapril and expression of organic anion transporting polypeptide 1 in zonal, isolated rat hepatocytes. *Drug Metab Dispos* 28:801-806.

Belz GG, Breithaupt-Grogler K, and Osowski U (2001) Treatment of congestive heart failure-current status of use of digitoxin. *Eur J Clin Invest* 31:10-17.

Bergwerk AJ, Shi X, Ford AC, Kanai N, Jacquemin E, Burk RD, Bai S, Novikoff PM, Stieger B, Meier PJ, Shuster VL and Wolkoff AW (1996) Immunologic distribution of an organic anion transport protein in rat liver and kidney. *Am J Physiol* 271: G231-G238.

Cattori V, van Montfoort JE, Stieger B, Landmann L, Meijer DKF and Hagenbuch B (2001) Localization of organic anion transporting polypeptide 4 (Oatp4) in rat liver and comparison of its substrate specificity with Oatp1, Oatp2, and Oatp3. *Plügers Arch – Eur J Physiol* 443:188-195.

Doherty JE and Perkins WH (1962) Studies with tritiated digoxin in human subjects after intravenous administration. *Am Heart J* 63:528-536.

Fromm MF, Kim RB, Stein CM, Wilkinson GR, and Roden DM (1999) Inhibition of P-glycoprotein-mediated drug transport: A unifying mechanism to explain the interaction between digoxin and quinidine. *Circulation* 99:552-557.

Goresky CA, Bach GG, and Nadeau BE (1975) Red cell carriage of label. Its limiting effect on the exchange of materials in the liver. *Circ Res* 36:328-351.

Guo GL and Klaassen CD (2001) Protein kinase C suppresses rat organic anion transporting polypeptide 1- and 2-mediated uptake. *J Pharmacol Exp Ther* 299:551-557.

Hagenbuch N, Reichel C, Stieger B, Cattori V, Fattinger KE, Landmann L, Meier PJ, and Kullak-Ublick GA (2001) Effect of phenobarbital on the expression of bile salt and organic anion transporters of rat liver. *J Hepatol* 34:881-887.

Harrison LI and Gibaldi M (1976) Pharmacokinetics of digoxin in the rat. *Drug Metab Dispos* 4:88-93.

Hinderling PH (1984) Kinetics of partitioning and binding of digoxin and its analogues in the subcompartments of blood. *J Pharm Sci* 73:1042-1053.

Hsiang B, Zhu Y, Wang Z, Wu Y, Sasseville V, Yang WP, and Kirchgessner TG (1999) A novel human hepatic organic anion transporting polypeptide (OATP2). Identification of a liver-specific human organic anion transporting polypeptide and identification of rat and human hydroxymethylglutaryl-CoA reductase inhibitor transporters. *J Biol Chem* 274:37161-37168.

Kullak-Ublick GA, Hagenbuch B, Stieger B, Wolkoff AW, and Meier PJ (1994) Functional characterization of the basolateral rat liver organic anion transporting polypeptide. *Hepatology* 20:411-416.

Kullak-Ublick GA, Ismair MG, Stieger B, Landmann L, Huber R, Pizzagalli F, Fattinger K, Meier PJ, and Hagenbuch B (2001) Organic anion-transporting polypeptide B (OATP-B) and its functional comparison with three other OATPs of human liver. *Gastroenterology* 120:525-533.

Kusuhara H, Sekine T, Utsunomiya-Tate N, Tsuda M, Kojima R, Cha SH, Sugiyama Y, Kanai Y, and Endou H (1999) Molecular cloning and characterization of a new multispecific organic anion transporter from rat brain. *J Biol Chem* 274:13675-13680.

Lau YY, Wu CY, Okochi H, and Benet LZ (2004) Ex situ inhibition of hepatic uptake and efflux significantly changes metabolism: hepatic enzyme-transporter interplay. *J Pharmacol Exp Ther* 308:1040-1045.

Lindros KO and Pentïlla KE (1985) Digitonin-collagenase perfusion for efficient separation of periportal or perivenous hepatocytes. *Biochem J* 228:757-760.

Liu L and Pang KS (2005) The roles of transporters and enzymes in hepatic drug processing. *Drug Metab Dispos* 33:1-9.

Lowry OH, Rosebrough NJ, Farr AL, and Randall RJ (1951) Protein measurement with the Folin phenol reagent. *J Biol Chem* 193:265-275.

Meier PJ and Stieger B (2002) Bile salt transporters. *Annu Rev Physiol* 64:635-661.

Meister A (1985) Glutamine synthetase from mammalian tissues. *Meth Enzymol* 113:185-199.

Noé B. Hagenbuch B, Stieger B, and Meier PJ (1997) Isolation of a multispecific organic anion and cardiac glycoside transporter from rat brain. *Proc Natl Acad Sci USA* 94:10346-10350.

Novikoff PM, Cammer TL, Oda H, Wolkoff AW, and Satir P (1996) Three-dimensional organization of rat hepatocyte cytoskeleton: relation to the asialoglycoprotein endocytosis pathway. *J Cell Sci* 109:21-32.

Okudaira K. Sawada Y, Sugiyama Y, Iga T, and Hanano M (1988) Effects of basic drugs on the hepatic transport of cardiac glycosides in rats. *Biochem Pharmacol* 37:2949-2955.

Oinonen T and Lindros KO (1995) Hormonal regulation of the zonated expression of cytochrome P-450 3A in rat liver. *Biochem J* 309:55-61.

Pang KS, Lee WF, Cherry WF, Yuen V, Accaputo J, Fayz S, Schwab AJ, and Goresky CA (1988) Effects of perfusate flow rate on measured blood volume, disse space, intracellular water space, and drug extraction in the perfused rat liver preparation: characterization by the multiple indicator dilution technique. *J Pharmacokinet Biopharm* 16:595-632.

Pang KS and Rowland M (1977) Hepatic clearance of drugs. I. Theoretical considerations of a "well-stirred" model and a "parallel tube" model. Influence of hepatic blood flow, plasma and blood cells binding, and the hepatocellular enzymatic activity on hepatic drug clearance. *J Pharmacokinet Biopharm* 5:625-653.

Pang KS and Stillwell RN (1983) An understanding of the role of enzyme localization of the liver on metabolite kinetics: a computer simulation. *J Pharmacokinet Biopharm* 11:451-468.

Pang KS, Wang PJ, Chung AF, and Wolkoff AW (1998) The modified dipeptide enalapril, an angiotensin converting enzyme (ACE) inhibitor, is transported by the rat liver organic anion transport protein (oatp1). *Hepatology* 28:1341-1346.

Reichel C, Gao B, van Montfoort J, Cattori V, Rahner C, Hagenbuch B, Stieger B, Kamisako T, and Meier PJ (1999) Localization and function of the organic anion-transporting polypeptide Oatp2 in rat liver. *Gastroenterology* 117:688-695.

Rodin SM and Johnson BF (1988) Pharmacokinetic interactions with digoxin. *Clin Pharmacokinet* 15:227-244.

Salphati L and Benet LZ (1999) Metabolism of digoxin and digoxigenin digitoxosides in rat liver microsomes: involvement of cytochrome P4503A. *Xenobiotica* 29:171-185.

Schinkel AH, Wagenaar E, van Deemter L, Mol CAAM, and Borst P (1995) Absence of mdr1a P-glycoprotein in mice affects tissue distribution and pharmacokinetics of dexamethasone, digoxin and cyclosporine A. *J Clin Invest* 96:1698-1705.

Shitara Y, Sugiyama D, Kusuhara H, Kato Y, Abe T, Meier PJ, Itoh T, and Sugiyama Y (2002). Comparative inhibitory effects of different compounds on rat oatpl (slc21a1)- and Oatp2 (Slc21a5)-mediated transport. *Pharm Res* 19:147-153.

Sirianni GL and Pang KS (1997) Organ clearance concepts: new perspectives on old principles. *J Pharmacokinet Biopharm* 25:449-470.

Tirona R and Pang KS (1996) Sequestered endoplasmic reticulum space for sequential metabolism of salicylamide: Coupling of hydroxylation and glucuronidation. *Drug Metab Dispos* 24: 821-833.

Tirona RG and Pang KS (1999) Bimolecular glutathione conjugation of ethacrynic acid and efflux of the glutathione adduct by periportal and perivenous rat hepatocytes. *J Pharmacol Exp Ther* 290: 1230-1241.

Tirona RG, Tan E, Meng LJ, Novikoff PM, Wang PJ, Wolkoff AW, Kim RB, and Pang KS (2000) Oatp2 is functionally distributed throughout the rat liver lobule and is a high affinity transporter of digoxin and sulfolithocholyltaurine (SLCT). *Hepatology* 32: 436A Abstr #1108.

Wirth KE and Frolich JC (1974) Effect of spironolactone on excretion of ^{3}H-digoxin and its metabolites in rats. *Eur J Pharmacol* 29:43-51.

FOOTNOTES

This work was supported by the Medical Research Council of Canada (MT-15657, MOP36457, and MOP65417 for K.S.P.), and the NIH (DK23026 for A.W.W.; CA06576 for P.M.N.).

Present address: Division of Clinical Pharmacology, Vanderbilt University, Nashville, TN 37232, USA (R.G.T.); Drug Metabolism, Merck & Co., InC., Rahway, NJ 07065, USA (E.T.)

Send reprint requests to: Dr. K. Sandy Pang, Faculty of pharmacy, University of Toronto, 19 Russell St., Toronto, Ontario, Canada M5S 2S2. E-mail: ks.pang@utoronto.ca

LEGENDS FOR FIGURES

Figure 1. HPLC tracings of Dg3, Dg2 and other metabolites Dg1 and Dg0 with unlabeled elution (upper panel) and radioelution in perfusate (middle panel) and bile (lower panel), respectively.

Figure 2. Exchange of substrate between rbc and plasma where f_{rbc} is the unbound fraction in rbc, which, when multiplied to the total concentration in rbc, C_{rbc}, yields $C_{rbc,u}$ or unbound drug concentrations in rbc. $C_{p,b}$ and $C_{p,u}$, are bound and unbound concentrations in plasma. Interchange between the unbound drug species is denoted by the rate constants, k_{rp} and k_{pr} that relates to unbound drug species, and k'_{rp} is used for $f_{rbc}\,k_{rp}$ since binding within rbc is unknown. The unbound fraction in plasma, f_p, is 0.64.

Figure 3. Two compartment models with elimination from central (A) and peripheral (B) compartment, in which k_{10} (or k_{20}) = k_e + k_m.

Figure 4. Physiologically-based pharmacokinetic (PBPK) models presenting recirculating rat liver perfusion with KHB (A) or 20% rbc-1% albumin (B). The liver tissue was divided into 3 zones (PP zone, middle zone and PV zone) according to the hepatic acinus physiology. CL_{ini}, CL_{efi}, $CL_{int,meti}$, and $CL_{int,seci}$ were assigned to different zones. $Dg2_L$ was the total formation of Dg2, which included Dg2 in reservoir, bile and liver tissue. The rbc partitioning parameters, k'_{rp} and k_{pr}, and protein binding parameter, f_p, from *in vitro* study were integrated into the PBPK model for fitting and simulation (B).

Figure 5. Rates of uptake by PP and PV isolated rat hepatocytes (mean ± SD) for digoxin at 37°C (n = 4): the lines represented fitted lines based on Equation 1 with an optimal weighting scheme of $1/observation^2$.

Figure 6. Western blotting of Oatp2 and Oatp1 from membrane fragments of PP and PV isolated rat hepatocytes. Note the even distribution of the immunodetectable proteins, and

confocal immunofluorescent microscopy of Oatp2 in periportal (PP) and perivenous (PV) regions of the rat liver.

Figure 7. Western blotting of Pgp from membrane fragments of PP and PV isolated rat hepatocytes which showed the even distribution of Pgp in periportal (PP) and perivenous (PV) regions of the rat liver.

Figure 8. Lack of concentration-dependent binding of digoxin to 1% or 2% BSA. Binding was modest and independent of the albumin concentration – 1 or 2%. The unbound fraction in plasma averaged 0.64 ± 0.03.

Figure 9. Fits of the data (n=3, mean ± SD) to model (Figure 2) after admixture of 40%-rbc, 1%-albumin perfusate to 0%-rbc and 1%-albumin perfusate containing [^{3}H]- and unlabeled digoxin. The numbers next to the fitted curves were the resultant blood concentrations. The optimized fit of the entire data set was achieved with a weighting scheme of 1/observation^2. The fit yielded on and off rate constants, k_{pr} (0.468 ± 0.021 min^{-1}) and k'_{rp} (1.81 ± 0.12 min^{-1}). Solid symbols are concentrations in rbc and open symbols are concentrations in plasma perfusate.

Figure 10. Fits of the data of KHB-perfused livers to compartmental models. (A) Data of Dg3 in reservoir ($Dg3_R$) and bile ($Dg3_{bile}$) were fit to two-compartment models with elimination from central (dash line) and peripheral (solid line) compartments (Figure 3). (B) The metabolite, Dg2 was found in both perfusate (solid circle) and bile (open circle), and the Dg2 amounts formed predicted from modeling were higher than the summed amount of Dg2 observed (solid triangle).

Figure 11. Fits of the data of rbc-alb-perfused livers to compartmental models. (A) Data of Dg3 in reservoir ($Dg3_R$) and bile ($Dg3_{bile}$) were fit to two-compartment models with elimination from central (dash line) and peripheral (solid line) compartments (Figure 3).

(B) The metabolite, Dg2 was found in both perfusate (solid circle) and bile (open circle), and the Dg2 amounts formed predicted from modeling were higher than the summed amount of Dg2 observed (solid triangle).

Figure 12. Fits of the data of Dg3 in reservoir ($Dg3_R$) and bile ($Dg3_{bile}$) to PBPK model (Figure 4) in KHB-perufsed (A) and rbc-alb-perfused (B) livers. The solid triangle symbols are summed amounts of Dg2 in reservoir and bile (% dose) that were underestimations of the total Dg2 formed ($Dg2_{total}$).

Figure 13. Simulations of the effect of flow rate (A) or binding (B) on Dg3 in reservoir ($Dg3_R$) and bile ($Dg3_{bile}$) and total Dg2 formation ($Dg2_{total}$) with the PBPK model (Figure 4B), based on parameter values for the rbc-alb-perfused livers (Table 4, middle column, and metabolic activity was evenly distributed). (A) The flow rate was changed from 10 ml/min (solid line) to 40 ml/min (dash-dot line). (B) The on and off binding constants for digoxin with red cell were set as zero ($k'_{rp} = k_{pr} = 0$) (—— ▪ ▪ ——), and binding to BSA was absent ($f_p = 1$) (— — —).

Figure 14. Simulations of the effect of doubling the CL_{in} (A), CL_{ef} (B), $CL_{int,met}$ (C), and $CL_{int,sec}$ (D) on Dg3 in reservoir ($Dg3_R$) and bile ($Dg3_{bile}$) and total Dg2 formation ($Dg2_{total}$) with PBPK model (Figure 4B), based on the parameter values from rbc-alb-perfused livers (Table 4, middle column, even distribution of $CL_{int,met}$). The changes from the original, controlled condition (——) were denoted as (—— ▪ ——).

JPET Fast Forward. Published on June 30, 2005 as DOI: 10.1124/jpet.105.088039
This article has not been copyedited and formatted. The final version may differ from this version.

Table 1: Lack of difference in uptake of digoxin by periportal and perivenous isolated rat hepatocytes in which the kinetics were best described by saturable and nonsaturable components (fitted with a weighting scheme of 1/observation^2)

	K_m [a] (nM)	V_{max} [a] (pmol/min/mg)	PS_{uptake} [b] (µl/min/mg)	CL_{uptake} [c] (µl/min/mg)
Periportal Hepatocytes (n=4)	180 ± 112	13 ± 8	9.2 ± 1.3	83 ± 29
Perivenous Hepatocytes (n=4)	390 ± 406	18 ± 4.9	10.7 ± 2.5	111 ± 80

[a] Saturable component
[b] Nonsaturable or linear uptake clearance
[c] Total hepatocyte uptake clearance (V_{max}/ K_m + PS_{uptake})

JPET Fast Forward. Published on June 30, 2005 as DOI: 10.1124/jpet.105.088039
This article has not been copyedited and formatted. The final version may differ from this version.

Table 2: Equilibrium values of digoxin unbound fractions for albumin and rbc binding

	20% rbc-1% Albumin Perfusate
Unbound fractions in plasma perfusate, f_p (1 % and 2 % albumin in perfusate) 0.01 to 100 μM digoxin	0.64 ± 0.03
Blood to plasma concentration ratio, C_b/C_p (for 0.02 to 20 μM digoxin)	1.04 ± 0.12
Red blood cell to blood concentration ratio, C_{rbc}/C_b (for 0.02 to 20 μM digoxin)	1.03 ± 0.12[a]
f_b	0.615[b]
k'_{rp} (min^{-1})	1.81 ± 0.12[c]
k_{pr} (min^{-1})	0.468 ± 0.021[c]

[a] Obtained according to Eq. 4
[b] Equal to $f_p/(C_b/C_p)$
[c] Obtained from fitting of C_{rbc} and C_p data (Eqs. 3 and 4)

JPET Fast Forward. Published on June 30, 2005 as DOI: 10.1124/jpet.105.088039
This article has not been copyedited and formatted. The final version may differ from this version.

Table 3: Comparison of pharmacokinetic parameters in KHB- and rbc-alb-perfused livers and fits of data to compartmental models (Figure 3) to arrive at the microconstants: k_{12}, k_{21}, k_e, k_m, k_{10}, and k_{20}. The optimal weighting scheme of unity was used.

	KHB- Perfused Livers	Rbc-Alb-Perfused Livers (20% rbc-1% Albumin)
Rat weight (g)	292 ± 3	327 ± 28*
Liver weight (g)	11.2 ± 1.4	12.3 ± 2.0
Hematocrit	0	0.14 ± 0.02*
Flow rate (ml/min)	40 ± 0	10 ± 0
Recovery		
Perfusate volume (% initial volume)	89 ± 5	91 ± 2
Radioactivity (% dose at 3 hour)		
Total bile	39 ± 17	25 ± 13
Bile: Dg3	11 ± 8	5 ± 2
Bile: Dg2	19 ± 10	14 ± 8
Total Perfusate	16 ± 5	28 ± 18
Perfusate: Dg3	11 ± 1	23 ± 13
Perfusate: Dg2	3 ± 2	5 ± 5
Liver tissue	38 ± 27	18 ± 1
Total recovery	93 ± 19	71 ± 13
AUC (from trapezoidal method)	7985 ± 2374	12362 ± 6938
$CL_{liver,tot}$	0.192 ± 0.049	0.123 ± 0.061
$CL_{liver,tot}/f_b$	0.192 ± 0.049	0.200 ± 0.098
Elimination from Central Compartment		
k_{12} (min^{-1})	0.379 ± 0.273[a]	0.141 ± 0.128
k_{21}(min^{-1})	0.137 ± 0.152	0.242 ± 0.224
k_{10} (min^{-1})	0.017 ± 0.006	0.0089 ± 0.0035
k_e (min^{-1})	0.0039 ± 0.0026	0.0007 ± 0.0003*
k_m (min^{-1})	0.013 ± 0.004	0.0082 ± 0.0032
MSC	16.5 ± 0.52	13.3 ± 0.71*
$CL_{liver,met}$ (ml/min/g)	0.185 ± 0.049	0.105 ± 0.052
$CL_{liver,ex}$ (ml/min/g)	0.059 ± 0.045	0.009 ± 0.005
$CL_{liver,tot}$ (ml/min/g)	0.244 ± 0.082	0.114 ± 0.057*
$CL_{liver,tot}/f_b$ (ml/min/g)	0.244 ± 0.082	0.185 ± 0.093
E	0.066 ± 0.017	0.133 ± 0.052
$CL_{int,sec}$ (ml/min/g)	0.060 ± 0.047	0.015 ± 0.009
$CL_{int,met}$ (ml/min/g)	0.196 ± 0.054	0.198 ± 0.103
Elimination from peripheral compartment		
k_{12} (min^{-1})	0.349 ± 0.288	0.171 ± 0.115
k_{21}(min^{-1})	0.190 ± 0.169	0.321 ± 0.196
k_{20} (min^{-1})	0.008 ± 0.006	0.018 ± 0.004*
k_e (min^{-1})	0.0017 ± 0.0015	0.0014 ± 0.0004
k_m (min^{-1})	0.0062 ± 0.0060	0.016 ± 0.004*
MSC	13.6 ± 2.85	13.2 ± 0.86
$CL_{liver,met}$ (ml/min/g)	0.140 ± 0.069	0.108 ± 0.045
$CL_{liver,ex}$ (ml/min/g)	0.058 ± 0.050	0.010 ± 0.005
$CL_{liver,tot}$ (ml/min/g)	0.198 ± 0.111	0.117 ± 0.051
$CL_{liver,tot}/f_b$ (ml/min/g)	0.198 ± 0.111	0.191 ± 0.083
E	0.053 ± 0.023	0.138 ± 0.043*
$CL_{int,sec}$ (ml/min/g)	0.059 ± 0.052	0.016 ± 0.009
$CL_{int,met}$ (ml/min/g)	0.146 ± 0.052	0.203 ± 0.091

[a] SD of mean, n=4

* $P < 0.05$ parameters in rbc-alb-perfused livers compared with those in KHB-perfused livers

JPET Fast Forward. Published on June 30, 2005 as DOI: 10.1124/jpet.105.088039
This article has not been copyedited and formatted. The final version may differ from this version.

Table 4: Assigned and fitted parameters to zonal model shown in Figure 4, based on the fit to the average data

	KHB-Perfused Livers	Rbc-Alb-Perfused Livers (20% rbc-1% Albumin)	Forced Fitting
Q (ml/min/g)	3.58	0.811	
Hct	0	0.142	
V_R (ml/g)	14.6 [a]	12.2	
V_S (ml/g)	0.149 [b]	0.149	
V_L (ml/g)	0.663 [c]	0.663	
k'_{rp} (min^{-1})	0	1.81	
k_{pr} (min^{-1})	0	0.468	
f_p	1	0.64	
CL_{in} (ml/min/g)	12.1 [d]	12.1	12.1
CL_{ef} (ml/min/g)	8.52 ± 54.0 [e] (9.28 ± 177) [f]	14.3 ± 388 (14.1 ± 204)	11.4 ± 776 (16.0 ± 262)
$CL_{int,met}$ (ml/min/g)	0.143 ± 0.901 (0.153 ± 2.91)	0.202 ± 5.49 (0.197 ± 2.84)	0.127 ± 8.66 (0.226 ± 3.70)
$CL_{int,sec}$ (ml/min/g)	0.054 ± 0.345 (0.059 ± 1.13)	0.017 ± 0.469 (0.017 ± 0.250)	0.025 ± 1.68 (0.046 ± 0.744)
f_t	0.018 ± 0.116 (0.017 ± 0.321)	0.051 ± 1.40 (0.052 ± 0.749)	0.034 ± 2.33 (0.019 ± 0.311)

[a] Mean of reservoir volume normalized to averaged liver weight
[b] Sinusoidal blood volume of liver, taken from Pang et al., 1988
[c] Cellular water space of liver, taken from Pang et al., 1988
[d] Calculated from data of Table 1, the data were scaled-up with the scaling factor(α/β; where α is 1.25×10^8 cells/g liver and β is 1×10^6 cells/mg protein)
[e] Fitted parameters when the metabolic activity, $CL_{int,met}$, was distributed heterogeneously (10%:30%:60% of total intrinsic clearance at zones 1, 2 and 3, respectively)
[f] Fitted parameters when $CL_{int,met}$ was distributed homogeneously in zones 1, 2 and 3

Table 5: Sensitivity of digoxin clearance to flow, binding, transport or intrinsic clearances: simulations with the PBPK model (control conditions: Q = 10 ml/min, with binding to red cells k'_{rp} = 1.81 min^{-1} k_{pr} = 0.468 min^{-1} for the rbc-alb-perfused livers) (Table 4)

	Control Condition	Changes						
		Q = 40 ml/min	$k'_{rp} = k_{pr} = 0$	$k'_{rp} = k_{pr} = 0$ $f_p = 1$	2 x CL_{in}	2 x CL_{ef}	2 x $CL_{int,met}$	2 x $CL_{int,sec}$
Hepatic clearance $CL_{liver,tot}$ (ml/min/g)	0.114	0.123	0.132	0.196	0.207	0.059	0.198	0.122
Metabolic clearance $CL_{liver,met}$ (ml/min/g)	0.105	0.113	0.122	0.180	0.190	0.055	0.190	0.104
Biliary clearance $CL_{liver,ex}$ (ml/min/g)	0.009	0.010	0.011	0.016	0.017	0.005	0.008	0.018
$CL_{liver,met}$ /$CL_{liver,ex}$	11.4	11.4	11.4	11.4	11.4	11.4	22.7	5.7

JPET Fast Forward. Published on June 30, 2005 as DOI: 10.1124/jpet.105.088039
This article has not been copyedited and formatted. The final version may differ from this version.

Table 6: The effects of zonal heterogeneity of influx/efflux transport, metabolism and secretion on clearances in digoxin hepatic disposition: simulations with the PBPK zonal model (Figure 4B)

	Control Condition CL_{in} = 12.1 ml/min/g CL_{ef} = 14.1 ml/min/g $CL_{int,met}$=0.197 ml/min/g $CL_{int,sec}$ = 0.017 ml/min/g	Assigned metabolic or secretory intrinsic clearances		
		5x $CL_{int,met}$ 50x $CL_{int,sec}$	100x $CL_{int,met}$ 500x $CL_{int,sec}$	0.1x $CL_{int,sec}$
Best condition				
$CL_{liver,tot}$ (ml/min/g)	0.11378 (AAA)[a]	0.5064 (AAA)	0.7653 (AAA)	0.10620 (AAC)
	0.11377 (AAC)	0.5061 (ACB)	0.7649 (AAC)	0.10620 (AAA)
	0.11377 (AAB)	0.5061 (ABC)	0.7649 (AAB)	0.10620 (AAB)
$CL_{liver,met}$ (ml/min/g)	0.10480 (AAB)	0.3118 (CCB)	0.6592 (CCB)	0.10530 (AAB)
	0.10458 (AAA)	0.3085 (ACB)	0.6424 (ACB)	0.10527 (AAA)
	0.10436 (AAC)	0.2947 (AAB)	0.6308 (CAB)	0.10525 (AAC)
$CL_{liver,ex}$ (ml/min/g)	0.00977 (ABC)	0.2826 (CBC)	0.4642 (CBC)	0.00098 (ABC)
	0.00973 (CBC)	0.2798 (ABC)	0.4419 (ABC)	0.00098 (CBC)
	0.00969 (BBC)	0.2632 (ABA)	0.3845 (CBA)	0.00098 (BBC)
Worst condition				
$CL_{liver,tot}$ (ml/min/g)	0.10867 (CBB)	0.4427 (CBB)	0.7356 (BCC)	0.10170 (CBB)
	0.10868 (BCC)	0.4427 (BCC)	0.7356 (CBB)	0.10171 (BCC)
	0.10916 (CBA)	0.4719 (CBA)	0.7464 (BCA)	0.10175 (CBA)
$CL_{liver,met}$ (ml/min/g)	0.09986 (CBC)	0.2064 (CBC)	0.2878 (CBC)	0.10081 (CBC)
	0.09987 (CBA)	0.2167 (CBA)	0.3228 (ABC)	0.10081 (CBA)
	0.09988 (CBB)	0.2263 (ABC)	0.3620 (CBA)	0.10081 (CBB)
$CL_{liver,ex}$ (ml/min/g)	0.00879 (CBB)	0.1803 (CCB)	0.1223 (CCB)	0.00089 (CBB)
	0.00879 (BCC)	0.1891 (CAB)	0.1220 (CAB)	0.00089 (BCC)
	0.00880 (CAB)	0.1976 (ACB)	0.0978 (ACB)	0.00089 (CAB)

[a] The three letters denote the distribution patterns of influx/efflux, metabolism, and secretory activities, with A denoting even distribution, B denoting 10%:30%:60% of total activity, and C denoting 60%:30%:10% of total activity in zones 1, 2, and 3, respectively

JPET Fast Forward. Published on June 30, 2005 as DOI: 10.1124/jpet.105.088039
This article has not been copyedited and formatted. The final version may differ from this version.

GLOSSARY

A_2	Dg3 amount in peripheral compartment
A_{bile} and A_{met}	Amount of Dg3 excreted into bile and metabolized, respectively
AUC	Area under the blood concentration-time curve of Dg3
C_1	Dg3 concentration in central compartment (compartmental modeling)
C_R (or $Dg3_R$)	Dg3 concentration, in the reservoir
$C_{rbc,R}$ (or $Dg3_{rbc,R}$)	Dg3 concentration in rbc, in the reservoir
$C_{p,R}$ (or $Dg3_{p,R}$)	Dg3 concentration in plasma, in the reservoir
C_{rbci} (or $Dg3_{rbci}$)	Dg3 concentration in red blood cell in sinusoid, in i^{th} zone (1, 2, or 3)
C_{pi} (or $Dg3_{pi}$)	Dg3 concentration in sinusoidal plasma, in i^{th} zone (1, 2, or 3)
C_{Li} (or $Dg3_{Li}$)	Dg3 concentration in liver tissue in i^{th} zone (1, 2, or 3)
$CL_{liver,tot}$	Total hepatic clearance
$CL_{liver,ex}$ and $CL_{liver,met}$	Biliary clearance and hepatic metabolic clearance, respectively
CL_{ini} and CL_{efi}	Basolateral influx and efflux clearance, of the i^{th} zone (1, 2, or 3), respectively
$CL_{int,seci}$ and $CL_{int,meti}$	Secretory intrinsic clearance and metabolic intrinsic clearance, of the i^{th} zone (1, 2, or 3), respectively
CL_{uptake}	First-order hepatocyte uptake clearance
$Dg2_{Li}$	"Effective" total Dg2 concentration formed in liver tissue in i^{th} zone (1, 2, or 3)

JPET Fast Forward. Published on June 30, 2005 as DOI: 10.1124/jpet.105.088039
This article has not been copyedited and formatted. The final version may differ from this version.

E	Hepatic extraction ratio
f_p, f_b, f_{rbc} and f_t	Unbound fractions of Dg3 in plasma, blood, red blood cells, and liver tissue, respectively
k_{10} and k_{20}	Elimination rate constants from central compartment, and from peripheral compartment, respectively
k_{12} and k_{21}	Intercompartment rate constants between compartment 1 and compartment 2
k_e and k_m	Rate constants for biliary excretion and metabolism formation from central compartment or from peripheral compartment, respectively
k_{pr} and k_{rp}	Exchange rate constants from plasma to rbc, and from rbc to plasma, respectively, whereby k'_{rp} equals the product $f_{rbc}\ k_{rp}$
$K_{m,i}$	Michaelis-Menten constant for the i^{th} transporter system
PS_{uptake}	Nonsaturable uptake clearance at sinusoidal membrane
Q and Q_{bile}	Total hepatic blood flow rate and bile flow rate, respectively
V_1	Volume of central compartment (compartment modeling)
V_R, V_S or V_L	Volume of reservoir, sinusoid, or liver tissue, respectively
V_{max}	Maximum velocity of the i^{th} transporter system

JPET Fast Forward. Published on June 30, 2005 as DOI: 10.1124/jpet.105.088039
This article has not been copyedited and formatted. The final version may differ from this version.

APPENDIX A

1) Two compartment model, with elimination from central compartment

For the rate of change of Dg3 in compartment 1

$$\frac{dC_1}{dt} = (k_{21}A_2 - (k_{12} + k_e + k_m)C_1V_1) / V_1 \quad \text{(A1)}$$

For the rate of change of Dg3 in compartment 2

$$\frac{dA_2}{dt} = k_{12}C_1V_1 - k_{21}A_2 \quad \text{(A2)}$$

For the cumulative amount of Dg3 excreted into bile

$$A_{bile} = \int k_eC_1V_1dt \quad \text{(A3)}$$

For the cumulative amount of Dg3 metabolized

$$A_{met} = \int k_mC_1V_1dt \quad \text{(A4)}$$

2) Two compartment model, with elimination from the peripheral compartment

For the rate of change of Dg3 in compartment 1

$$\frac{dC_1}{dt} = (k_{21}A_2 - k_{12}C_1V_1) / V_1 \quad \text{(A5)}$$

For the rate of change of Dg3 in compartment 2

$$\frac{dA_2}{dt} = k_{12}C_1V_1 - (k_{21} + k_e + k_m)A_2 \quad \text{(A6)}$$

For the cumulative amount of Dg3 excreted into bile

$$A_{bile} = \int k_eA_2dt \quad \text{(A7)}$$

For the cumulative amount of Dg3 metabolized

$$A_{met} = \int k_mA_2dt \quad \text{(A8)}$$

JPET Fast Forward. Published on June 30, 2005 as DOI: 10.1124/jpet.105.088039
This article has not been copyedited and formatted. The final version may differ from this version.

APPENDIX B

Mass balance equations of the physiologically-based pharmacokinetic (PBPK) zonal, liver model that described the disposition of Dg3 in rbc-albumin rat liver preparations (Figure 4B) with even distribution of $CL_{int,met}$.

For the rate of change of Dg3 in reservoir (whole blood, rbc, or plasma)

$$\frac{dC_R}{dt} = (QHctC_{rbc3} + Q(1-Hct)C_{p3} - QC_R) / V_R \quad \text{(B1)}$$

$$\frac{dC_{rbc,R}}{dt} = (k_{pr} f_p C_{p,R} V_R (1-Hct) - k'_{rp} C_{rbc,R} V_R Hct - QHctC_{rbc,R} + QHctC_{rbc3}) / (V_R Hct) \quad \text{(B2)}$$

$$\frac{dC_{p,R}}{dt} = (k'_{rp} C_{rbc,R} V_R Hct - k_{pr} f_p C_{p,R} V_R (1-Hct) - Q(1-Hct)C_{p,R} + Q(1-Hct)C_{p3}) / (V_R (1-Hct)) \quad \text{(B3)}$$

For the rate of change of Dg3 in zone 1 (rbc, plasma or liver tissue)

$$\frac{dC_{rbc1}}{dt} = (k_{pr} f_p C_{p1} \frac{V_S}{3}(1-Hct) - k'_{rp} C_{rbc1} \frac{V_S}{3} Hct - QHctC_{rbc1} + QHctC_{rbc,R}) / (\frac{V_S}{3} Hct) \quad \text{(B4)}$$

$$\frac{dC_{p1}}{dt} = (k'_{rp} C_{rbc1} \frac{V_S}{3} Hct - k_{pr} f_p C_{p1} \frac{V_S}{3}(1-Hct) - Q(1-Hct)C_{p1} + Q(1-Hct)C_{p,R} - f_p C_{p1} \frac{CL_{in}}{3} + f_t C_{L1} \frac{CL_{ef}}{3}) / (\frac{V_S}{3}(1-Hct)) \quad \text{(B5)}$$

$$\frac{dC_{L1}}{dt} = (f_p C_{p1} \frac{CL_{in}}{3} - f_t C_{L1} \frac{CL_{ef} + CL_{int,sec} + CL_{int,met}}{3}) / (\frac{V_L}{3}) \quad \text{(B6)}$$

For the rate of change of Dg3 in zone 2 (rbc, plasma or liver tissue)

$$\frac{dC_{rbc2}}{dt} = (k_{pr} f_p C_{p2} \frac{V_S}{3}(1-Hct) - k'_{rp} C_{rbc2} \frac{V_S}{3} Hct - QHctC_{rbc2} + QHctC_{rbc1}) / (\frac{V_S}{3} Hct) \quad \text{(B7)}$$

$$\frac{dC_{p2}}{dt} = (k'_{rp} C_{rbc2} \frac{V_S}{3} Hct - k_{pr} f_p C_{p2} \frac{V_S}{3}(1-Hct) - Q(1-Hct)C_{p2} + Q(1-Hct)C_{p1} - f_p C_{p2} \frac{CL_{in}}{3} + f_t C_{L2} \frac{CL_{ef}}{3}) / (\frac{V_S}{3}(1-Hct)) \quad \text{(B8)}$$

JPET Fast Forward. Published on June 30, 2005 as DOI: 10.1124/jpet.105.088039
This article has not been copyedited and formatted. The final version may differ from this version.

$$\frac{dC_{L2}}{dt} = (f_p C_{p2} \frac{CL_{in}}{3} - f_t C_{L2} \frac{CL_{ef} + CL_{int,sec} + CL_{int,met}}{3}) / (\frac{V_L}{3}) \quad \text{(B9)}$$

For the rate of change of Dg3 in zone 3 (rbc, plasma or liver tissue)

$$\frac{dC_{rbc3}}{dt} = (k_{pr} f_p C_{p3} \frac{V_S}{3}(1 - Hct) - k'_{rp} C_{rbc3} \frac{V_S}{3} Hct - QHctC_{rbc3} + QHctC_{rbc2}) / (\frac{V_S}{3} Hct) \quad \text{(B10)}$$

$$\frac{dC_{p3}}{dt} = (k'_{rp} C_{rbc3} \frac{V_S}{3} Hct - k_{pr} f_p C_{p3} \frac{V_S}{3}(1 - Hct) - Q(1 - Hct)C_{p3} + Q(1 - Hct)C_{p2} - f_p C_{p3} \frac{CL_{in}}{3} + f_t C_{L3} \frac{CL_{ef}}{3}) / (\frac{V_S}{3}(1 - Hct)) \quad \text{(B11)}$$

$$\frac{dC_{L3}}{dt} = (f_p C_{p3} \frac{CL_{in}}{3} - f_t C_{L3} \frac{CL_{ef} + CL_{int,sec} + CL_{int,met}}{3}) / (\frac{V_L}{3}) \quad \text{(B12)}$$

For the cumulative amount of Dg3 excreted into bile

$$A_{bile} = \int f_t (C_{L1} + C_{L2} + C_{L3}) \frac{CL_{int,sec}}{3} dt \quad \text{(B13)}$$

For the cumulative amount of Dg2 metabolized

$$A_{met} = \int f_t (C_{L1} + C_{L2} + C_{L3}) \frac{CL_{int,met}}{3} dt \quad \text{(B14)}$$

JPET Fast Forward. Published on June 30, 2005 as DOI: 10.1124/jpet.105.088039

Figure 1

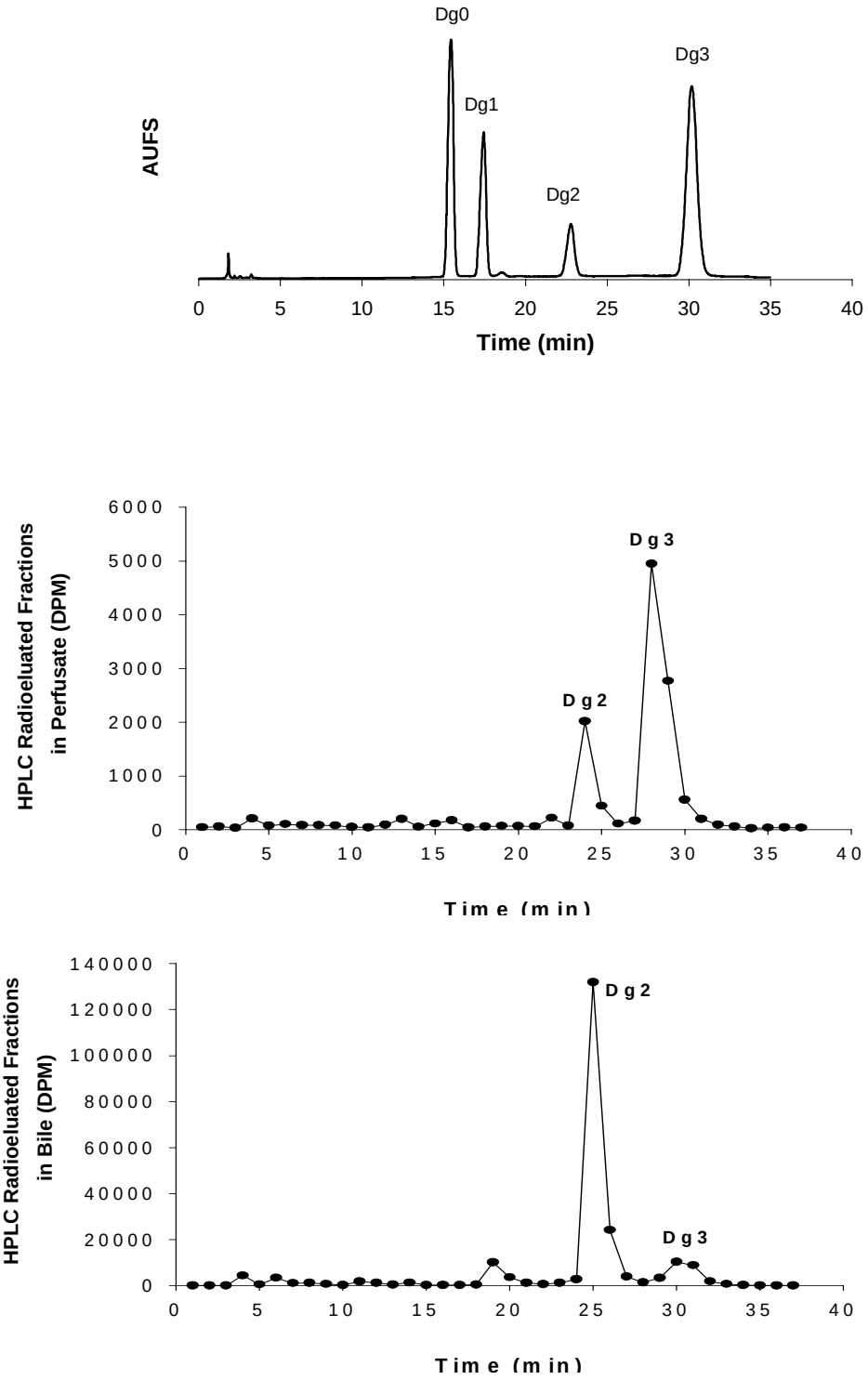

JPET Fast Forward. Published on June 30, 2005 as DOI: 10.1124/jpet.105.088039

Figure 2

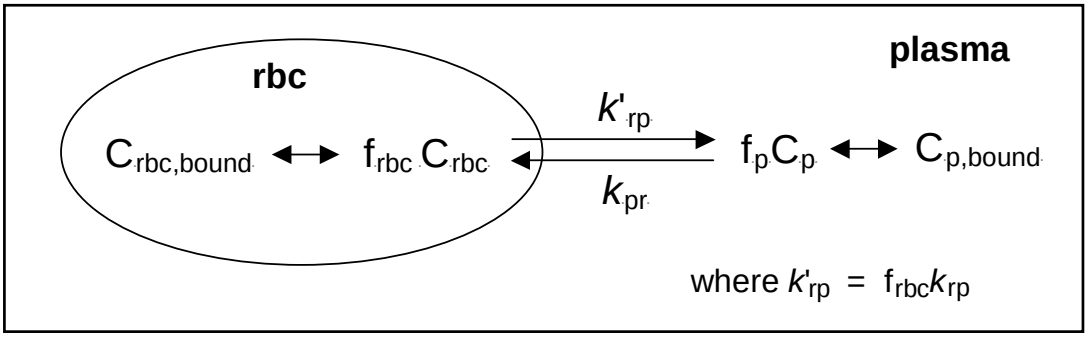

JPET Fast Forward. Published on June 30, 2005 as DOI: 10.1124/jpet.105.088039

Figure 3

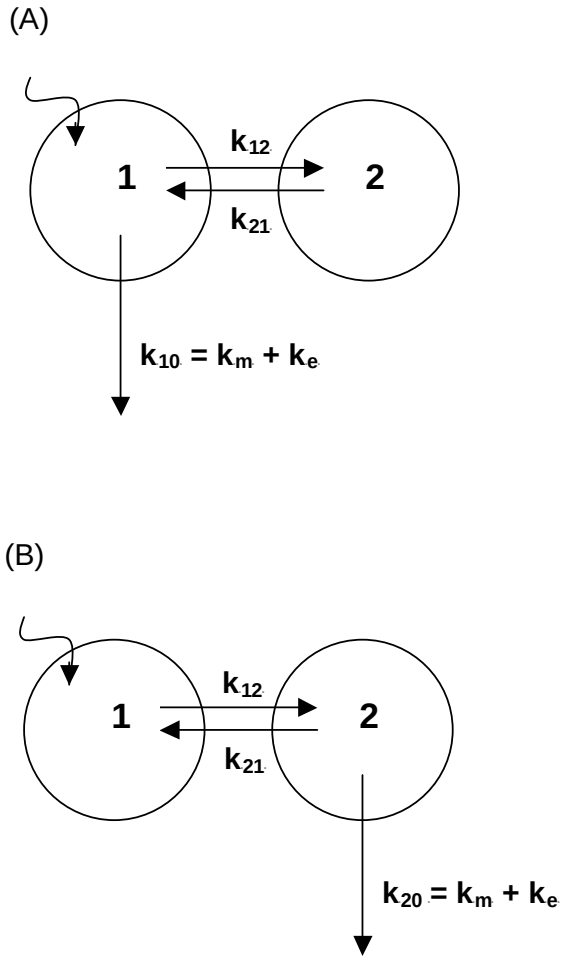

JPET Fast Forward. Published on June 30, 2005 as DOI: 10.1124/jpet.105.088039

Figure 4

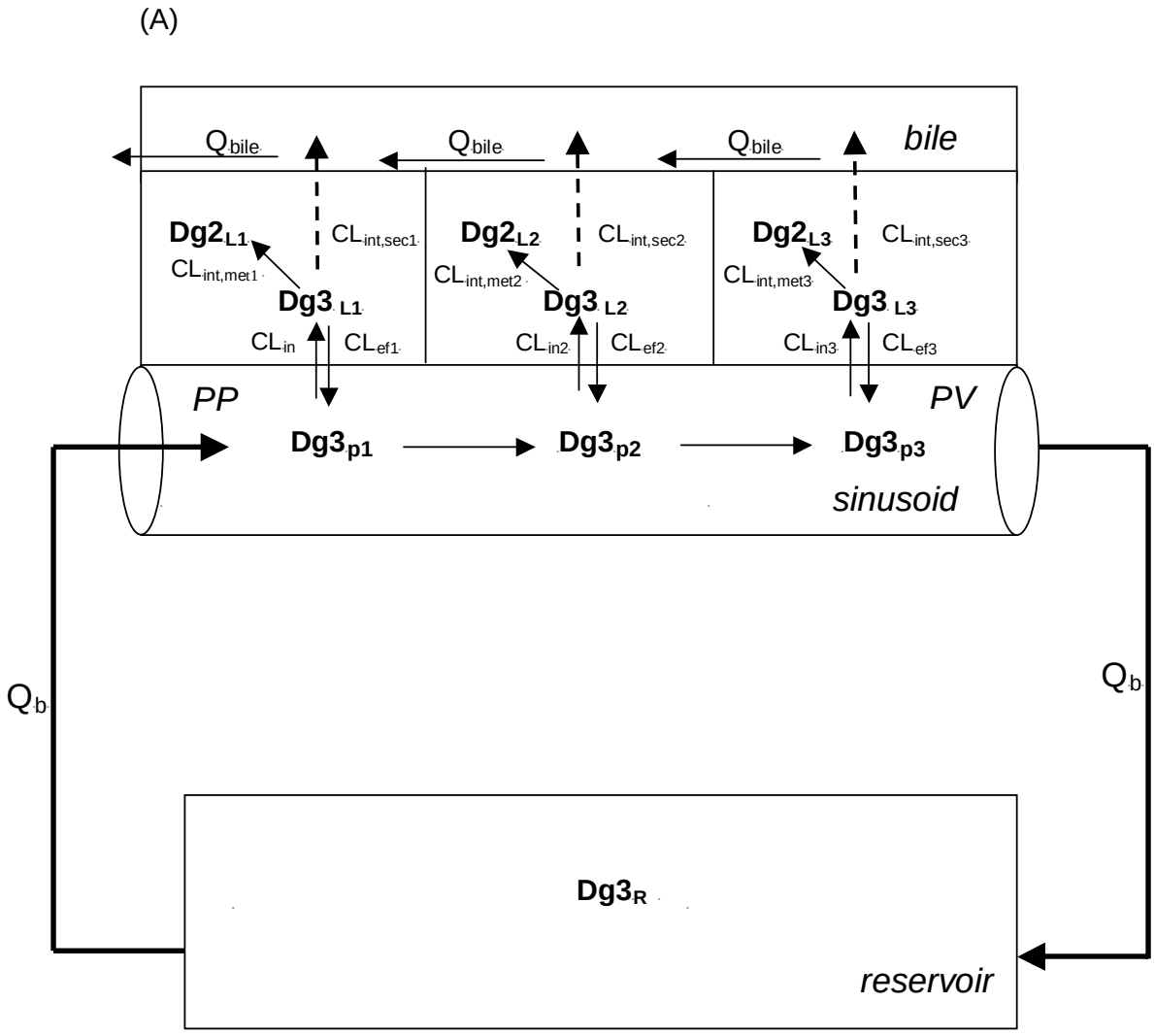

JPET Fast Forward. Published on June 30, 2005 as DOI: 10.1124/jpet.105.088039

Figure 4

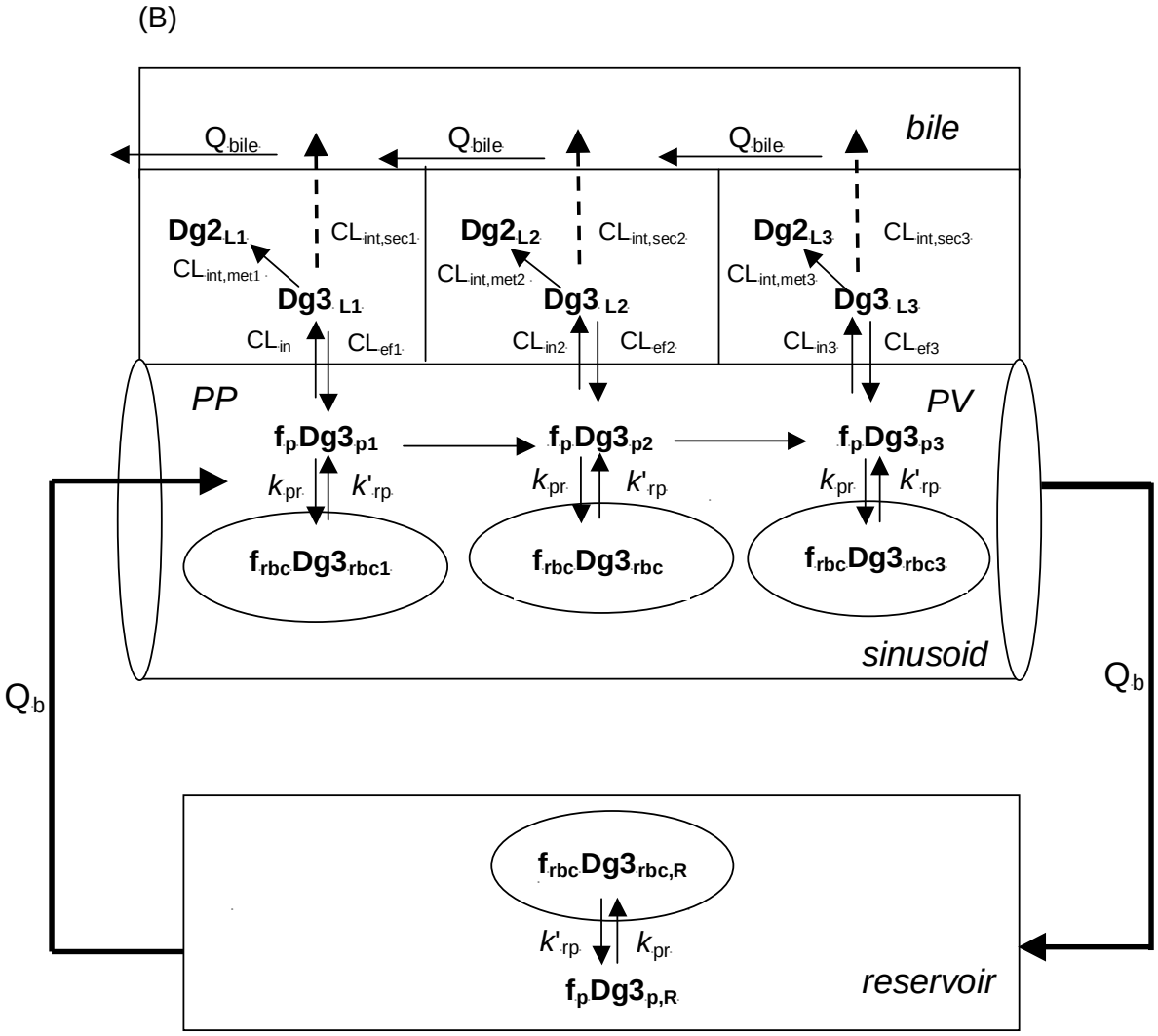

JPET Fast Forward. Published on June 30, 2005 as DOI: 10.1124/jpet.105.088039

Figure 5

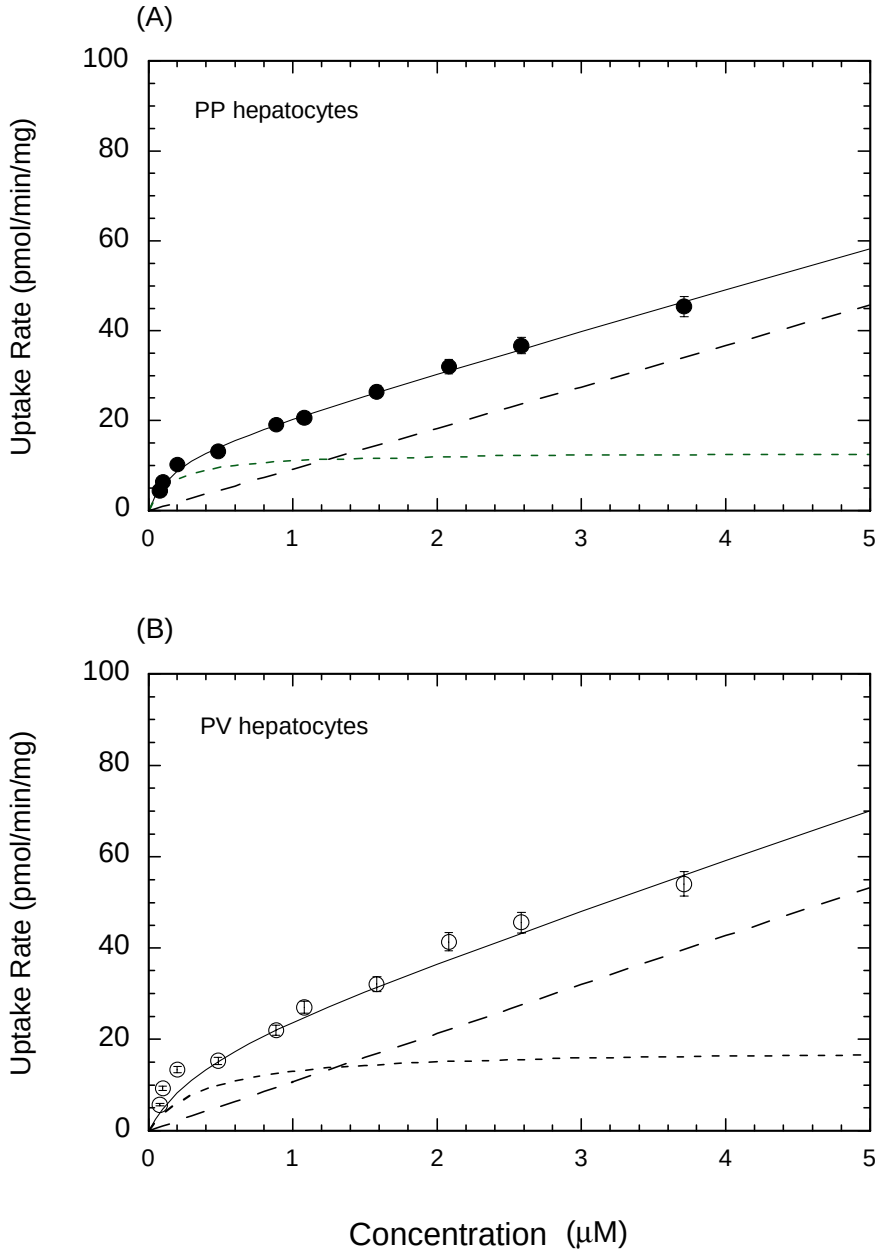

JPET Fast Forward. Published on June 30, 2005 as DOI: 10.1124/jpet.105.088039

Figure 6

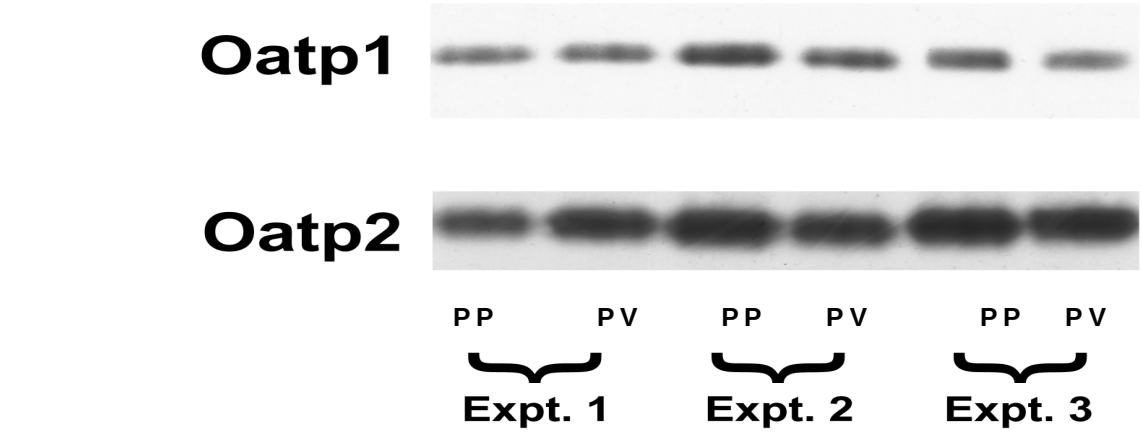

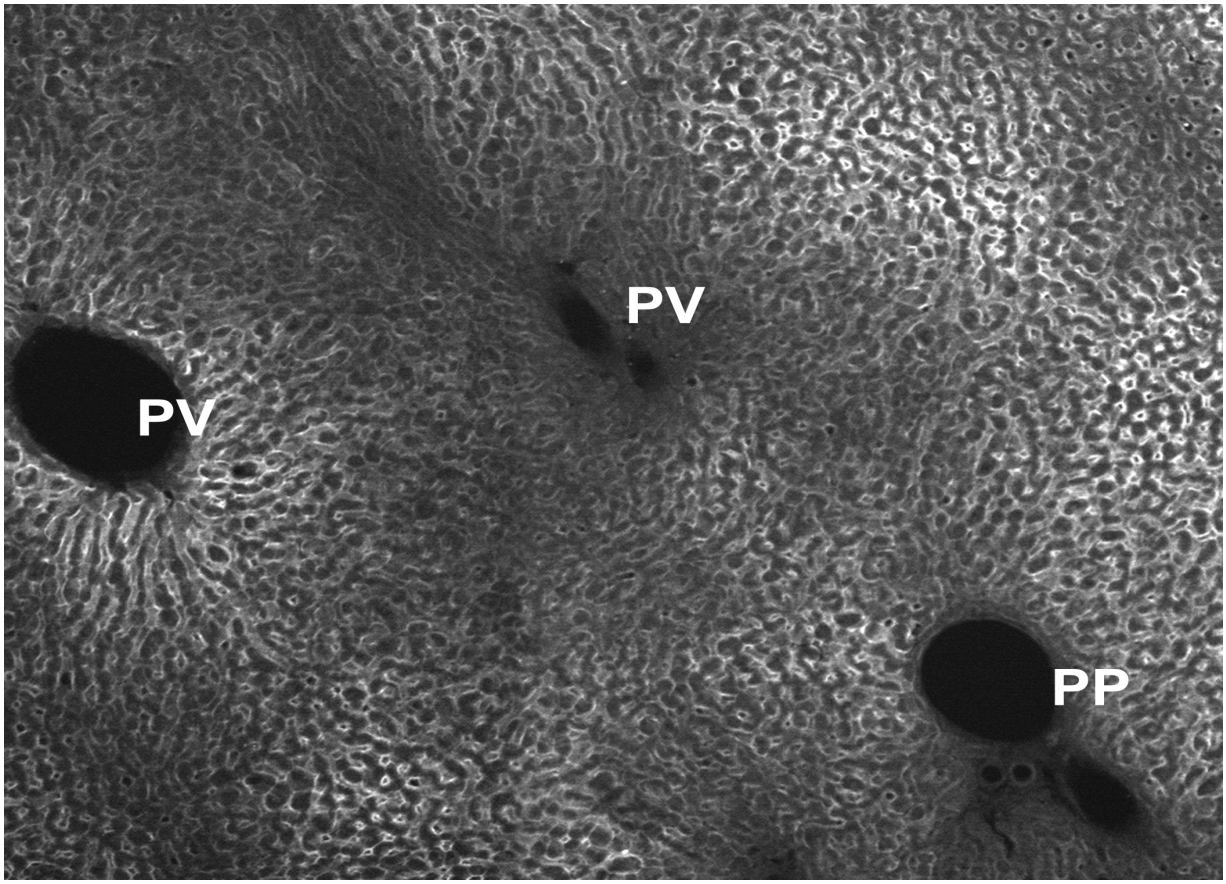

JPET Fast Forward. Published on June 30, 2005 as DOI: 10.1124/jpet.105.088039

Figure 7

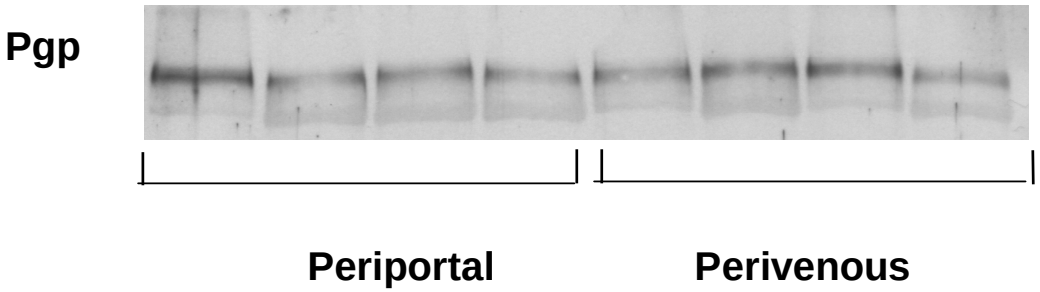

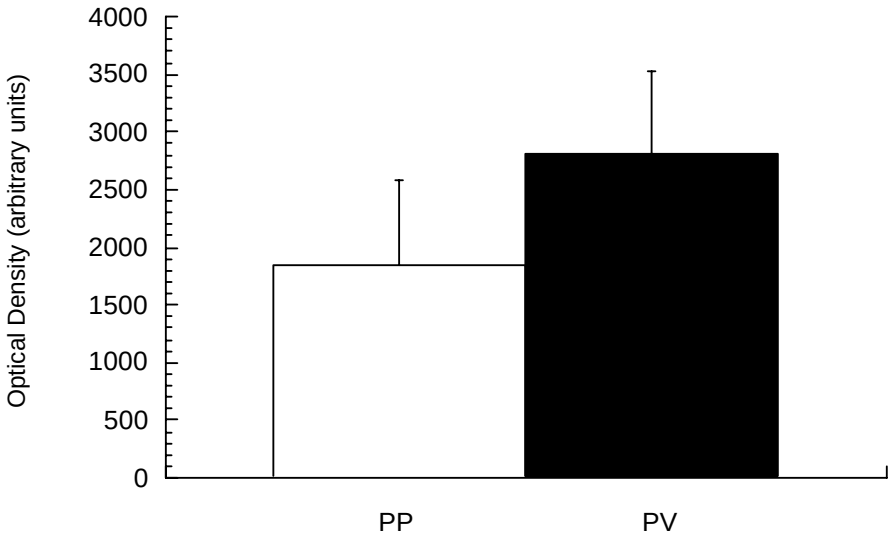

JPET Fast Forward. Published on June 30, 2005 as DOI: 10.1124/jpet.105.088039

Figure 8

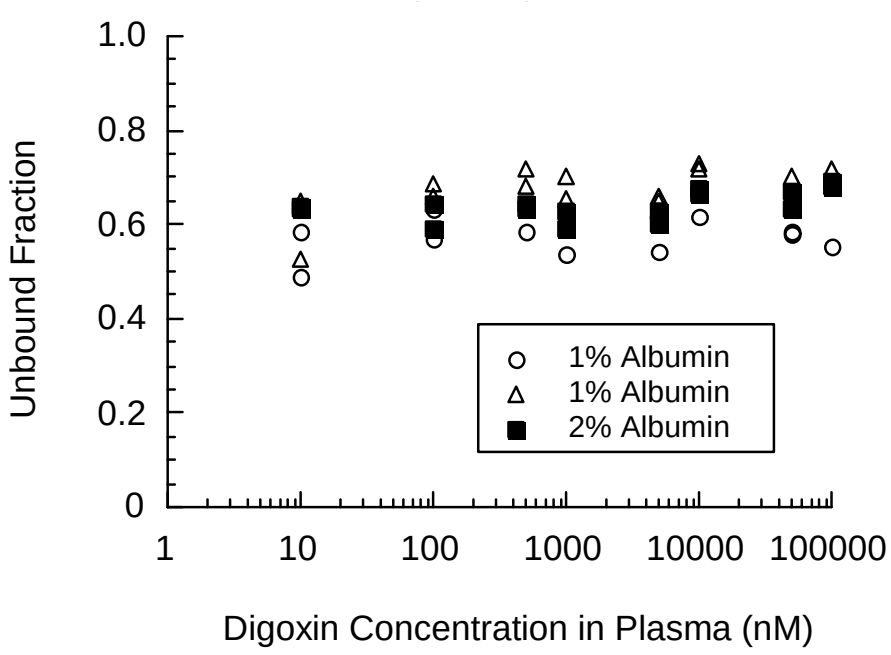

Figure 9

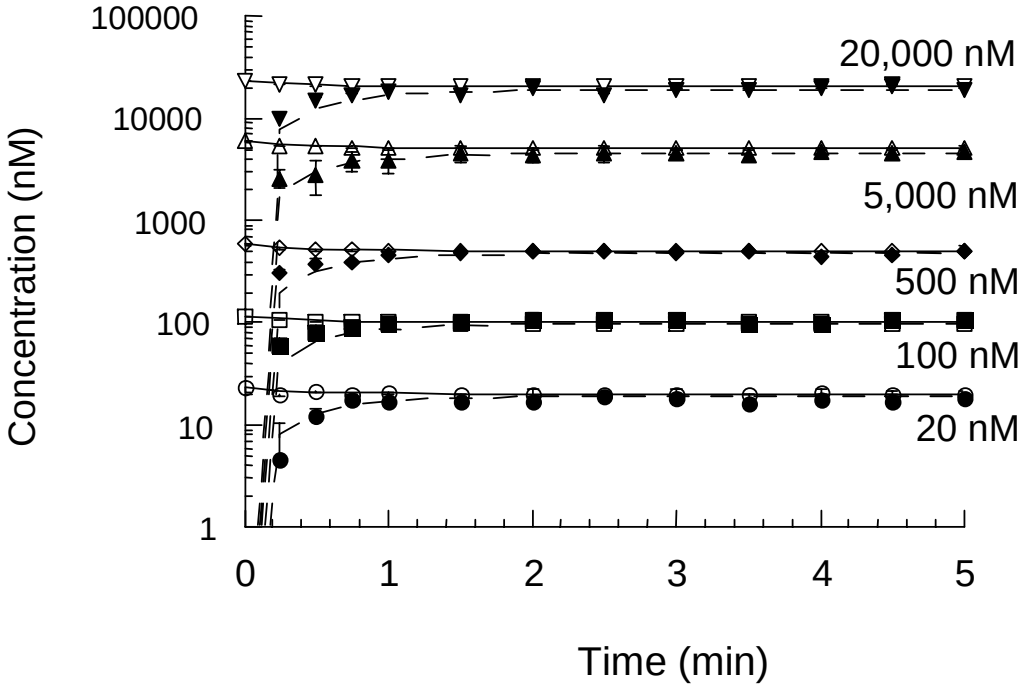

JPET Fast Forward. Published on June 30, 2005 as DOI: 10.1124/jpet.105.088039

Figure 10

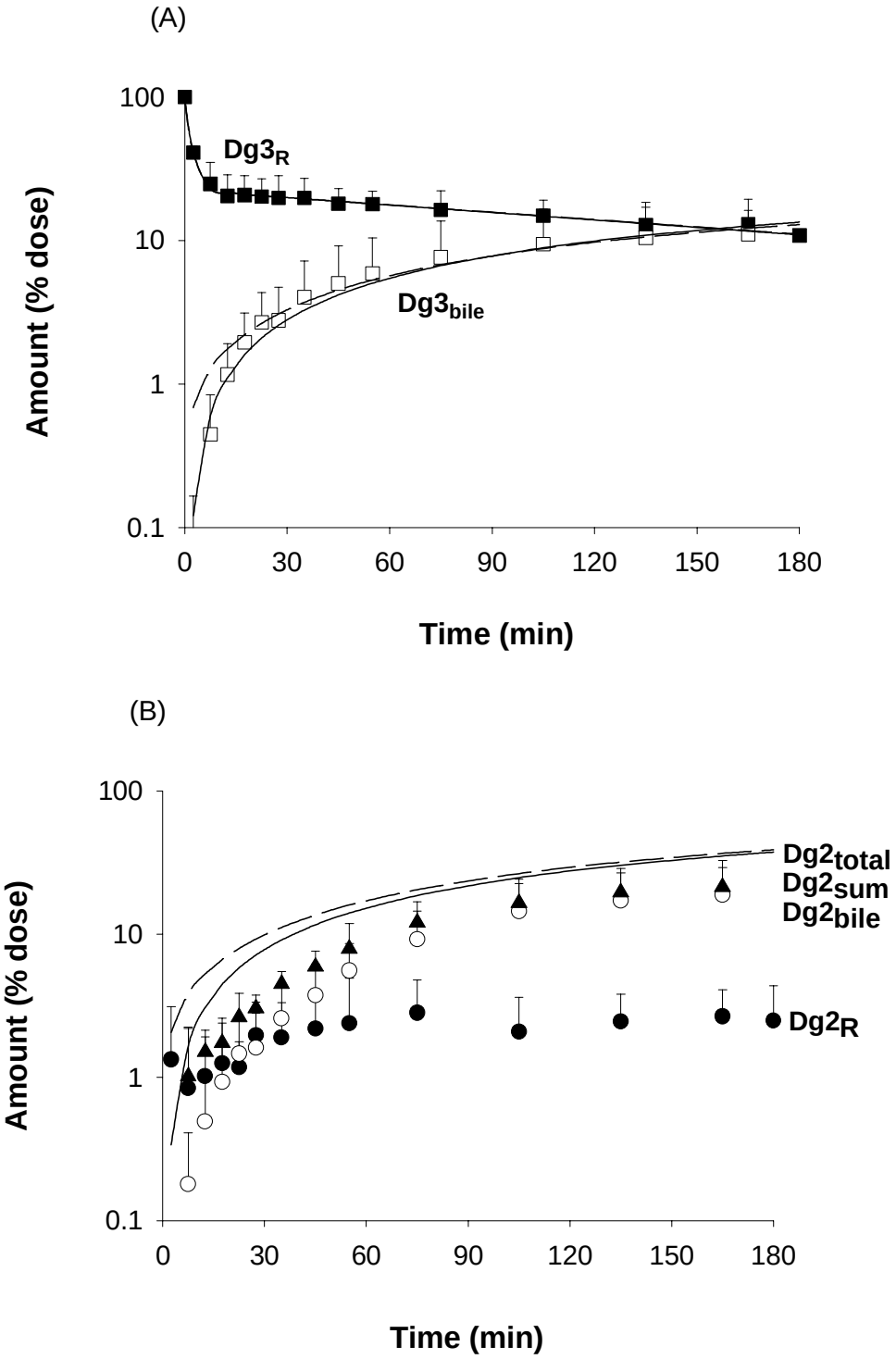

JPET Fast Forward. Published on June 30, 2005 as DOI: 10.1124/jpet.105.088039

Figure 11

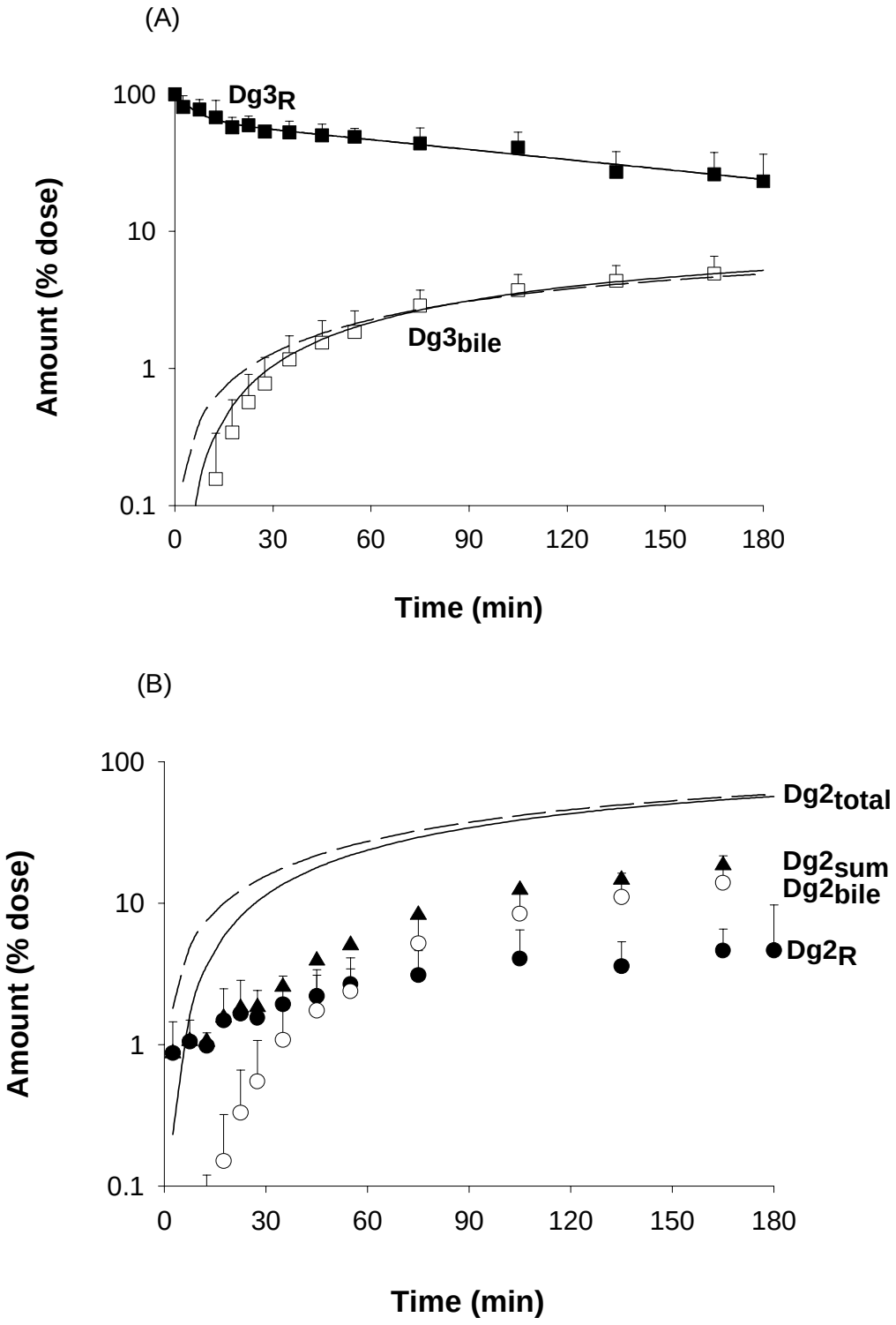

JPET Fast Forward. Published on June 30, 2005 as DOI: 10.1124/jpet.105.088039

Figure 12

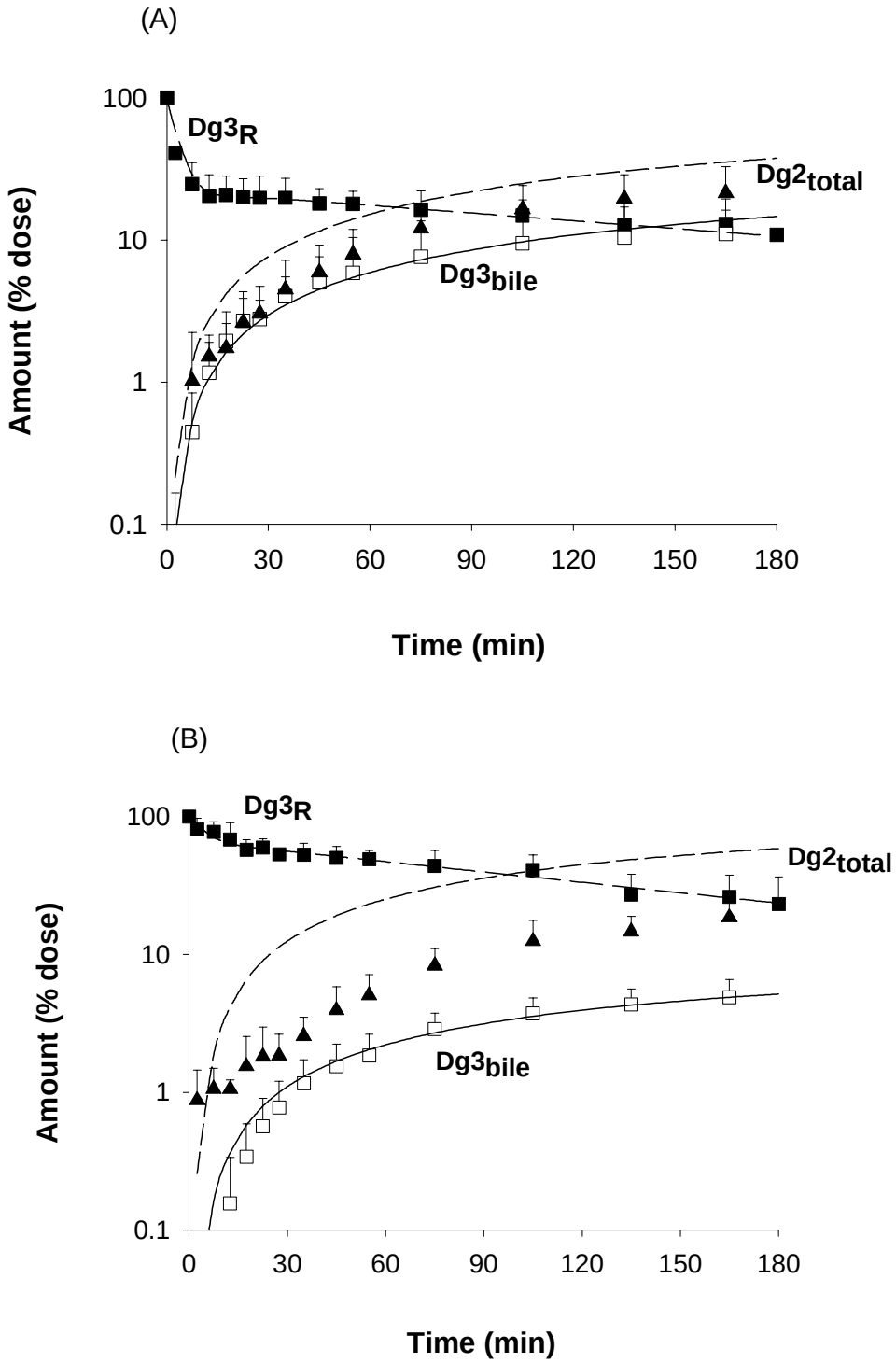

JPET Fast Forward. Published on June 30, 2005 as DOI: 10.1124/jpet.105.088039

Figure 13

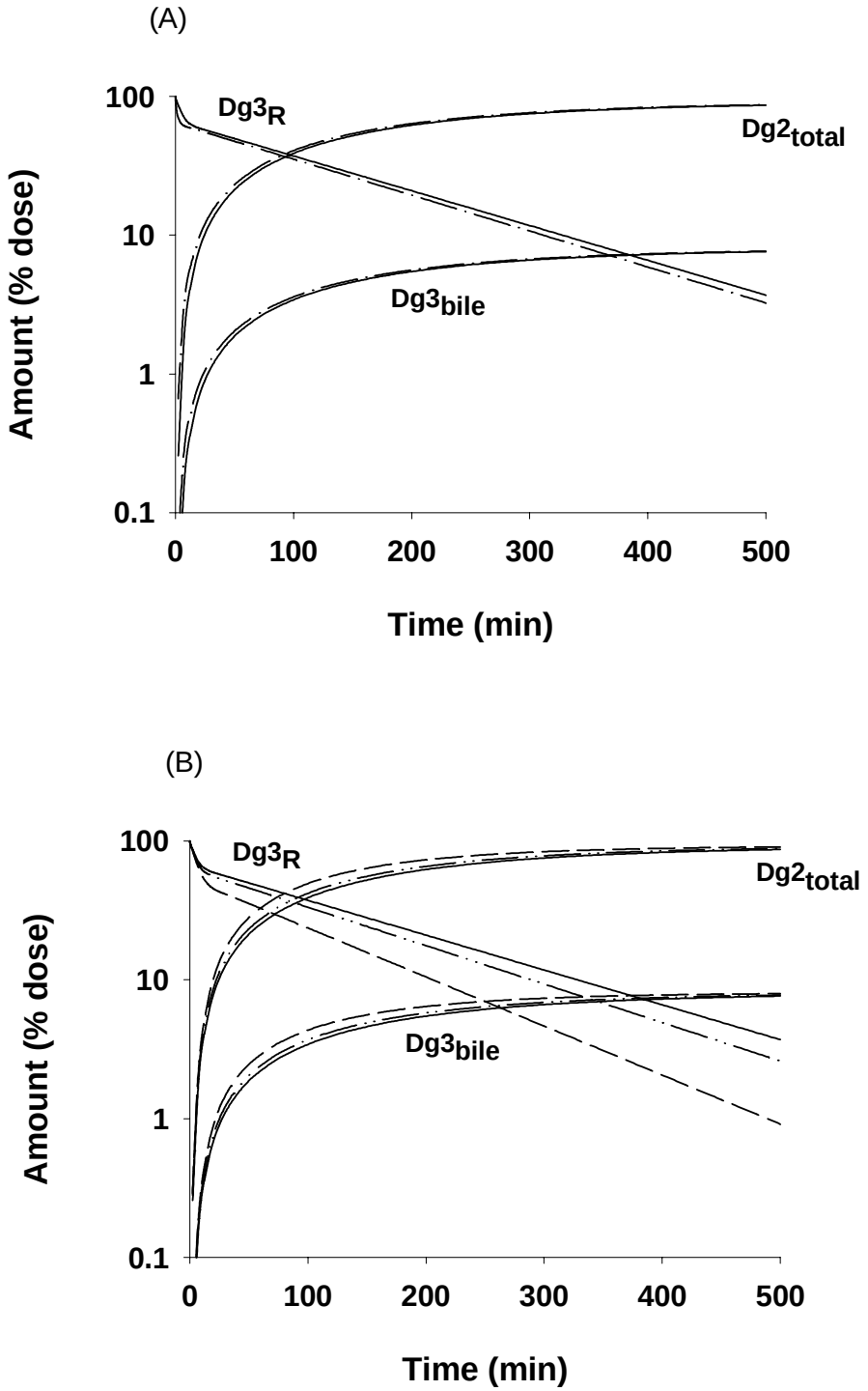

Figure 14